Engineering Applications of Artificial Intelligence 24 (2011) 278–294

Contents lists available at ScienceDirect

Engineering Applications of Artificial Intelligence

journal homepage: www.elsevier.com/locate/engappai

Energy conservation based fuzzy tracking for unmanned aerial vehicle missions under a priori known wind information

Georgios P. Kladis [a], John T. Economou [a,*], Kevin Knowles [a], Jimmy Lauber [b], Thierry-Marie Guerra [b]

[a] Intelligent Propulsion & Emissions Lab, Aeromechanical Systems Group, Cranfield University, Defence Academy of the United Kingdom, Shrivenham, Swindon, Wiltshire SN6 8LA, United Kingdom

[b] Laboratoire d'Automatique, de Mècanique et d' Informatique industrielles et Humaines, LAMIH, Universitè de Valenciennes, BP 311, Le Mont Houy, 59313 Valenciennes Cedex 9, France

ARTICLE INFO

Article history:
Received 12 February 2010
Received in revised form
26 July 2010
Accepted 14 October 2010
Available online 26 November 2010

Keywords:
Graph theory
Energy cost matrix
Pre-flight planning
Energy conservation
Parallel distributed compensation
Takagi–Sugeno fuzzy model
Linear matrix inequalities

ABSTRACT

The aim of this work is to include the navigation step for the waypoint-based guidance of a UAV system and to illustrate aspects such as tracking of the reference trajectory under wind presence, while conserving total energy requirements. The mission is represented utilising graph theory tools. The mathematical modelling of an aircraft controlled by an actuator surface is presented in terms of simple analytic relationships in order to simulate the actual horizontal motion of the vehicle. Its equivalence with a Tagaki–Sugeno (T-S) fuzzy system is illustrated that can aid the control methodology involved. Additionally, the advantages of utilising such an analysis is also stressed. The model formulated is an error posture model, that depends on current and reference posture. The control law is designed through parallel distributed compensation (PDC) and the gains are computed with the help of linear matrix inequalities (LMIs). Hence stability for the system is also guaranteed provided that the state variables are bounded in a priori known compact space. Moreover the energy requirements are described.

This article is contributing towards energy enhancing a UAV mission and generating safely-flyable trajectories to meet mission objectives. The control law used is calculated in the pre-flight planning and can be used in real time for any trajectory to be tracked under any environmental conditions. Provided that angular and linear velocities are bounded, the latter is feasible under the assumption that the magnitude of air speed is *small* compared to the ground velocity of the aerial vehicle. The methodology offers an improved visualisation to aid an analyst with the representation of a UAV mission through graph theory tools utilising energy requirements for the mission and fast computational schema using matrix analysis.

A simulation example of a UAV deployed from a source to reach a destination node under windy conditions is included to illustrate the analysis. The reference trajectory used is a piecewise Bezier–Bernstein curve referred to as the Dubins path.

1. Introduction

On board guidance and control systems are used to monitor flight performance. Apart from the time of arrival and endurance of flight they are also utilised to maintain updated fuel reserves. Presently, overall flight planning is performed on ground dispatch computers. However, it is crucial to be able to estimate, real-time, the fuel profile on board in order to increase automation and performance of the preflight planning when disturbances occur. In other words, wasting fuel due to unforecast disturbances can degrade the performance of the preflight planning mechanism. At the same end, if the time of arrival is available by a particular strategy then a fuel optimal trajectory can be possibly generated on-line with manipulation of flight parameters like speed, propulsion magnitude, angle, etc.

Existing research till recently, focused heavily on methods which improve the path planning algorithms. In particular, the optimum paths based on minimum distance or time travelled has been addressed from researches in Richards and How (2002) and Rathinam and Sengupta (2004a), among other interesting works. In practice, the optimum distance path solutions do not take into account the energy constraints. Without the energy utilisation the selected path may not be feasible or realisable. In other words, when disturbances occur in a path, such as an unforecast unfavorable wind, then the shortest distance path may not guarantee an energy optimum one. The latter was shown in work (Economou et al., 2007b) where the authors decoupled the problem of a shortest path from the Euclidean perspective and the energy one. In addition they proposed a methodology utilising energy graphs and pseudo-boolean expressions to describe the overall energy requirements. Consequently motivated by such an analysis there is a need to

* Corresponding author.
E-mail addresses: j.t.economou@cranfield.ac.uk (J.T. Economou), jimmy.lauber@univ-valenciennes.fr (J. Lauber).

0952-1976/$ - see front matter © 2010 Elsevier Ltd. All rights reserved.
doi:10.1016/j.engappai.2010.10.013

investigate the problem of navigation from the energy perspective rather than the shortest distance one.

Apart from the *Navigation* phase the pre-flight planning involves also the *Guidance* phase. In fact if energy routes are of interest the problem becomes threefold. Firstly, a predefined trajectory needs to be followed, the ground speed of the vehicle should be regulated and decision making should be performed in order to find a *minimum sense* path to follow that will fulfil mission objectives. Thus energy requirements should be described and then the path of optimum sense to reach a goal should be calculated. In the proposed analysis a graph theory formulation of the problem, introduced in Economou et al. (2007a, b) and Kladis et al. (2007), is combined with the physical and functional limitations of the vehicle with a focus on energy conservation of the involved flight path.

The tracking problem remains even nowadays a challenging area. Depending on the application domain, an adequate control law needs to be designed in order to fulfil mission objectives. Among many interesting approaches solving the tracking problem are those of Fliess et al. (1995) and Laumond (1998). Those are focused on the motion planning problem. However, their limitation lies in asymptotic tracking when the ground velocity of the vehicle becomes zero. Moreover, other works by Kanayama et al. (1991) and Klančar and Skrjanc (2007) suggested the combination of state feed-forward and feed-back control actions. The stability of the system was proved through a Lyapunov function and the gains were computed by linearisation of the tracking-error model to zero. Although there is potential in such approaches a serious drawback is with respect to their performance in real-time. The latter occurs due to the fact that the gains calculated that stabilise the system need to be updated and recalculated when the trajectory to be tracked is altered due to an event while in flight.

The approach proposed in this article, which is coupled with the routing problem, is based on the equivalent Takagi–Sugeno fuzzy model to the nonlinear error posture model of the vehicle's kinematics, introduced in earlier work (Tanaka et al., 1996). The control law used (parallel distributed compensation, PDC, Sugeno and Kang, 1986 and later improved by Wang et al., 1995) is computed utilising liner matrix inequality (LMI) techniques (Tanaka and Wang, 2001). The methodology proposed can be implemented for any type of reference trajectory provided that linear and angular velocities are bounded and $|V_w| \ll |V_g|$. $|V_w|$, $|V_g|$ are the magnitude of the wind and ground velocity, respectively. The latter can be interpreted with respect to the physical and functional limitations of the vehicle. The trajectory used in this work is the Dubins (1957) path. Additionally, disturbance rejection conditions are included in order to accommodate real world conditions. Stability is proven for any initial condition of the system for a priori known compact space of the state variables.

This article is contributing towards energy-enhancing a UAV mission and generating safely-flyable trajectories to meet mission objectives. The control law used is calculated in the pre-flight planning and can be used in real time for any trajectory. Additionally, it offers an improved visualisation to aid an analyst with the representation of a UAV mission through graph theory tools utilising energy requirements for the mission and fast computational schema using matrix analysis.

In this work preliminaries are addressed in Section 2. Those involve the graph theory tools. The vehicle's kinematics, the trajectory to be used, the model of environmental conditions and the description of the energy requirements are also included. Thereafter, in Section 3 the error posture model used and its equivalence to the Takagi–Sugeno (T–S) model are described. Additionally, the architecture of the controller and LMI conditions that stabilise the system are also included. Finally through a simulation example the analysis is illustrated in Section 4.2. In Section 5 concluding remarks are stated. Lastly an Appendix is added that includes the gains calculated for the control law for the T–S fuzzy model.

2. Preliminaries

2.1. Graph theory tools in the context of UAVs

In this section the graph theory preliminaries and the relevance to the waypoint-based formulation of the UAV mission are stated. Adopting the notation in Christofides (1975), a graph G is an ordered triplet (V,E,φ), where V is the set of vertices or nodes ($V=\{1,2,3,\ \ldots,V_{\max}\}$), E is the set of edges, ($E=\{c_1,c_2,\ \ldots,c_l\}$), which represent every possible connection created between a pair of nodes and φ the direction for every different element in the set of E, respectively, ($\varphi=\{(1,1),(1,2),\ldots,(i,j),\ldots,(j,i)\}$), where $i,j\in\{1,2,\ldots,V_{\max}\}$. A graph G can be represented in a form of the adjacency matrix $\mathbf{A}=[a_{ij}]$, where $\mathbf{A}\in\mathbb{R}^{nxn}$. For our cause *energy graphs* are utilised as suggested in earlier works (Economou et al., 2007b; Kladis et al., 2008a). The description of the energy requirements for the UAV mission is explained in Section 2.5.

In addition, properties included in Economou et al. (2007b) such as the flight adjacency matrix, the reachable matrix, the energy matrix bounded on perturbations, mission reachability matrix, etc., provide a solid framework for the use of graph theory in the context of unmanned aerial vehicles. Among them a useful graph theory property is concerned with reachability $\mathbf{R}=[r_{ij}]$. Its importance lies in the fact that through elementary calculations it can be decided whether or not a path is feasible prior to computing the optimum waypoint based sequence to reach a goal. The particular was also stressed in our earlier work (Kladis et al., 2007).

2.2. Modelling the motion of an aircraft

For the purpose of the simulations the kinematics model (1) is considered, for bank to bank turns under wind presence, with the necessary assumptions, as explained in Vinh (1995). Thus assuming that the thrust and the velocity vector are collinear (the thrust angle of attack becomes zero), the altitude and the ground velocity V_g are maintained constant (flight path angle and dV_g/dt becomes zero) then a full nonlinear aircraft model reduces to (1). This captures the most important key parameters for lateral motion of an electrically powered aircraft. In particular maintaining constant altitude can be assumed under realistic scenarios where the operational regime requires for the UAV to fly at an altitude within which there are no conflicting paths with flight traffic. Furthermore due to atmospheric properties a particular altitude can be fuel saving. Additionally, it can be assumed due to mission constraints (e.g. on reconnaissance missions the UAV needs to photograph a region in a stealthy manner). In practice, the point mass kinematics model (1) is valid only for small deviation of angles. Thus a more complex model, such as the one described in Stevens and Lewis (1992), can handle greater deviations since the coupling between variables is considered. However, the latter is beyond this work. An important reason is the fact that coordinated[1] bank to bank turns are taken into account for the UAV.

The motion of the point mass aircraft model (1) can be defined by the position coordinates x, y, the speed V_g, the heading angle θ and the mass m. Assuming a relatively short segment of flight path the weight of the fuel propelled aircraft, calculated as $W=mg$, can

[1] A coordinated turn in the horizontal plane is one in which there is no sideslip angle and the velocity vector is in the plane of symmetry containing the aerodynamic and the propulsive forces.

be considered constant. Instead, if an electrically actuated aircraft is considered its weight is maintained constant throughout the entire mission provided that the payload is not changed. g is the acceleration due to gravity. The equations of flight are

$$\frac{dx}{dt} = V_g\cos\theta + V_w\cos(\theta_w)$$

$$\frac{dy}{dt} = V_g\sin\theta + V_w\sin(\theta_w)$$

$$\frac{d\psi}{dt} = \frac{g}{V_g}\tan\varphi \tag{1}$$

where $\varphi \in [\varphi_{min},\varphi_{max}]$ is the roll angle (the angle between the vertical plane and the plane of symmetry of the aircraft). $Wind = (V_w,\theta_w)$ is the wind vector. Additionally, $V_w = N(0,\sigma)$ and $\theta_w = N(0,\xi)$. The N notation denotes properties of a Gaussian distribution. The weather conditions are a priori known with the help of range Doppler radars or anemometers placed at masts over buildings (when flying at low altitude). Thus the wind's velocity can be estimated and is assumed to be $|V_w| \ll |V_g|$. It is straightforward that if the previous condition does not hold then the aircraft cannot meet its objectives.

Assuming that wind disturbances are a priori known under a strategy then tracking of a predetermined path can be feasible. The tracking problem, under a priori known wind profile *Wind* in the global frame, can be formulated as to find the adequate input command φ to track a predefined trajectory denoted by vectors x_d^T and y_d^T in global frame. In other words, find φ such that $e_i = (x_{d_i},y_{d_i}) - (x_i,y_i) = 0$ as $t \to \infty$ where x, y vectors are the position coordinates of the displaced path due to the wind vector $Wind = (V_w,\theta_w)$. This falls under the category of tracking problems and is described in the next sections.

2.3. The Dubins path

Path planning is a geometric evolution of a curve and trajectory shaping is the time evolution of a curve. Path planning connects a starting to an end point by a path. These two points are characterized by the *poses* denoted as $A(x,y,\theta)$. Apart from producing a sequence of waypoints the path planner should design such a path that does not violate physical constraints of the vehicle. Those can entail minimum bank to bank turns, fuel consumption, propulsive limitations, flyable time, etc. In order for the path planner to produce a path $s(t)$ the poses and constraints should be known a priori.

Mathematically a path is represented by a curve, like a piecewise polynomial known as the Bezier–Bernstein curve referred to as the "*Dubins*" path (Dubins, 1957). The Dubins path is used in this work. Benefits of utilising such a trajectory can be found in previous work (Shanmugavel, 2007) for the interested reader. The path produced can be single or composite. Hence given the poses and constraints ϖ initially, the solution(s) ($s(t)$) can be formulated as follows:

$$P_{start}(x_{start},y_{start},\theta_{start}) \xrightarrow{s(t)} P_{final}(x_{final},y_{final},\theta_{final}),\varpi \tag{2}$$

The Dubins path comprises line segments and circular arcs of type CLC or CCC (C= Circular arc, L= Line segment) or another combination of the previous two. By the former two segments of the circumference of two circles are joined by their common tangent. By the latter, CCC is formed by three consecutive tangential circular arcs. The physical interpretation of the particular path is a combination of the shortest line for rectilinear motion and the shortest circular arc for turning. Relevant works utilising the Dubins path for path planning in a UAV application can be found in Rathinam and Sengupta (2004b), Allison and Hedrick (2005) and Shanmugavel (2007). Example trajectories for *CLC* paths with common external and internal tangents, respectively, are depicted in Fig. 2. The two waypoints depicted have poses of P_{start}(100, 100,80°) and P_{final}(150,150,45°). The Dubins path is constructed with the use of principles of Euclidean Geometry. The design procedure can be found in a thesis (Shanmugavel, 2007). Additionally in another thesis (Kladis, 2010) reasons for choosing such a trajectory can be found for the interested reader.

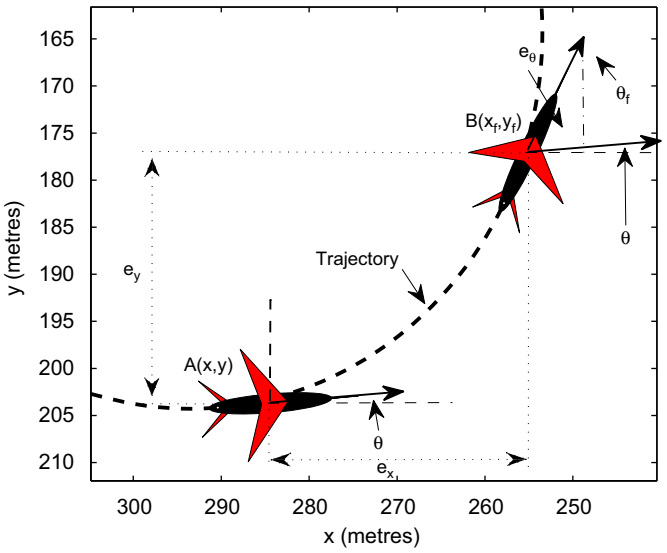

Fig. 1. Posture error $P(x_e,y_e,\theta_e)$ for an aerial vehicle in lateral motion.

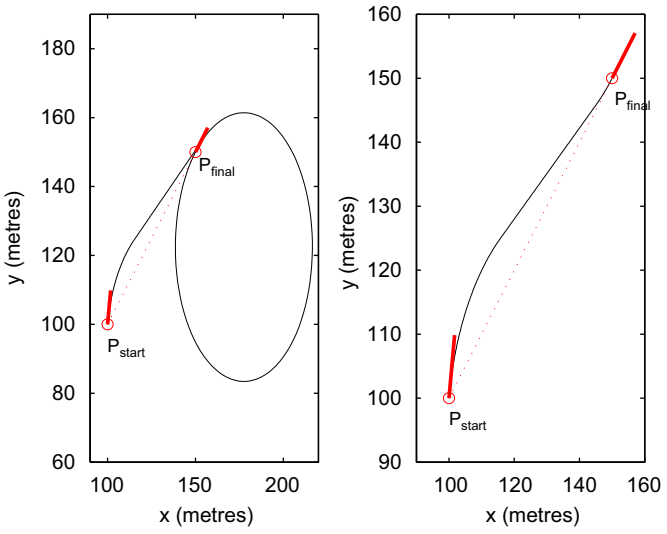

Fig. 2. Common external (left) and internal (right) tangent between two circular arcs. The solid red lines in source and destination waypoints depict the entry and exit heading angles at the particular poses. (For interpretation of the references to colour in this figure legend, the reader is referred to the web version of this article.).

It should be noted that for the previous poses there exist four different Dubins paths, the left to left turn (LSL), the left to right turn (LSR), the right to right turn (RSR) and the right to left turn (RSL). From the previous four trajectories for the node to node path the one that yields the minimum energy requirements is chosen and used in the energy cost matrix **P**. The latter is shown in the simulation example described later.

2.4. Model of environmental conditions

In nature, environmental conditions play an important role with respect to the flight conditions that birds and insects can fly,

let alone the flying conditions from micro-aerial vehicles to commercial aircraft. Hence conditions can impose a considerable challenge to their capability of flying (limitations, strength, etc.) to overcome such flight conditions to track a trajectory, for example. Hence under low-wind conditions insects can remain grounded. Similarly while worse environmental conditions occur larger insects, birds, etc. can become immobilised. Thus, it is valid to assume that in order for the aerial vehicle to fly then condition $|V_w| \ll |V_g|$ must be satisfied. The latter was also suggested in the work of Tennekes (1996) where a thorough list of flying speeds with respect to *Beaufort* wind scale (Table 1) indicated the wind conditions that aircraft, birds and insects can fly in and outlined the previous assumption.

The model of wind used in this work has two features: direction with respect to the global frame and magnitude. The weather map used is depicted in Fig. 5, where the arrows depict the direction of wind in the global frame and the contours the means the magnitude of wind is changing topologically within the map. The model used for the magnitude is assumed to be a multimodal distribution of the form:

$$V_w(x,y) = \sum_{i=1}^{n} \alpha_i e^{-((x-\mu_i^x)^2 + (y-\mu_i^y)^2/\beta_i^2\sigma_i^2)} \tag{3}$$

where $i=1,2,\ldots,n$, μ^x, μ^y, α, β and σ are the control variables of the environment defined by Eq. (3). Thus the environmental conditions (i.e magnitude of wind) to be used for each Dubins path (s_i) are determined by the interpolation of the path s_i and V_w. The heading angle of wind can be represented also by such a model, however, for simplicity, it is assumed constant for each node to node path.

Lastly the magnitude of wind profile considered later in the simulation scenario varies from 0 to 5 m/s wind speed. The latter lies in the interval of 0–3 on the Beaufort scale which is consistent with flying conditions for bees to human powered aircraft.

2.5. Energy requirements for mission

Adopting the terminology in our earlier work (Economou et al., 2007b) and motivated by Economou et al. (1999), where the mathematical background regarding the force Newtonian equations, the power and energy mathematical descriptions were proposed, the energy adjacency matrix $\Lambda \in \mathbb{R}^{nxn}$ for a UAV travelling at a constant speed u and impulse matrix $\mathbf{F}$ during time interval $\Delta_{i,j} = [t^0, t]$ for $\forall$ possible paths $\mathbf{\Lambda}[i,j]$, where all node-to-node paths are non-equal times $\underline{\Delta_{i,j}}$, is equal to $\mathbf{\Lambda} = [u. \int_{t_{i,j}^0}^{t_{i,j}} F_{i,j}(\tau)\, d\tau\, dt]$. The generalised energy cost matrix $\mathbf{\Lambda}$ for a graph $G(V,E)$ has the form $\mathbf{\Lambda} = [\min(p_{i,j}^*)]\ \forall i,j \in V$.

Each element $p_{i,j}^*$ represents the energy requirements for the trajectory connecting path $i \rightarrow j$ and yields the minimum cost. The trajectory is denoted by index $* \in \{1,2,3,4\}$. The previous is valid due to the fact that there are four trajectories that connect the adjacent nodes with poses $P_i(x_i,y_i,\theta_i)$ and $P_j(x_j,y_j,\theta_j)$ through their internal and external tangents. The latter occurred due to the heading constraint enforced in the particular poses, as mentioned in Section 2.3.

Thus element ρ_{ij} of the adjacency matrix $\mathbf{\Lambda}$ represents the energy demand, rather than distances, for the node to node sequence $(i \rightarrow j)$ and is calculated through the vehicle's kinematics which is illustrated in this section. The latter is performed provided that actuators and sensors of the aircraft are considered as an efficient and negligible part of the system. The atmospheric weather conditions are known from weather Doppler radars a priori. These conditions affect the forces acting on the known UAV airframe thus resulting in known energy path costs. Consequently, for a specific UAV deployed for a mission estimations of variables, such as forces applied, are known. Therefore the energy matrix is calculated. For a point mass object the total energy in terms of UAV model's parameters can be obtained from (4):

$$\begin{aligned} E_{Total} &= E_{\delta v v} + E_{\kappa \iota v} = mg\left(h + \frac{1}{2g}V_a^2\right) = mg\left(h + \frac{1}{2g}(\dot{x}^2 + \dot{y}^2)\right) \\ &= mg\left(h + \frac{1}{2g}(V_g^2 + 2V_g W_x \cos(\theta) + 2V_g W_y \sin(\theta) + W_x^2 + W_y^2)\right) \\ &= WE_s \end{aligned} \tag{4}$$

where $(W_x, W_y) = (V_w\cos(\theta_w), V_w\sin(\theta_w))$, h the altitude and V_a the actual velocity of the vehicle. Eq. (4) is valid ignoring stored energy such as fuel or electrical energy stored in power cells (batteries). E_s is termed *Specific Energy* and is a criterion to illustrate design performance which is decoupled from the mass of the vehicle. However, it acquires an offset with respect to the altitude the operations take place. Additionally the first derivative of the E_s coincides with the specific energy rate which is equal to

$$\frac{dE_s}{dt} = \frac{dh}{dt} + \frac{1}{g}\frac{dV_a}{dt}V_a \tag{5}$$

Table 1
Environmental conditions in which birds, insects and commercial aircraft can fly according to Tennekes (1996).

Wind speed (m/s)	Beaufort wind scale		
	Force	Description	
0.6	1	Light air	Butterflies
1			
2			
	2	Light breeze	Gnats, midges, damselflies
3			
4			
	3	Gentle breeze	Human-powered aircraft, flies, dragonflies
5			
6			
	4	Moderate breeze	Bees, Wasps, beetles, hummingbirds, swallows
8			
10	5	Fresh breeze	Sparrows, thrushes, finches, owls, buzzards
	6	Strong breeze	Blackbirds, crows
	7	Near gale	Gulls, falcons
20	8	Gale	Ducks, geese
	9	Strong gale	Swans, coots
	10	Storm	Sailplanes
30	11	Violent storm	Light aircraft
	12	Hurricane	

The energy rate is equal to

$$E_r = \frac{dE_{Total}}{dt} = W\frac{dE_s}{dt} + E_s\frac{dW}{dt} \tag{6}$$

Integrating Eq. (4) results in the overall energy requirements for the UAV mission. Thus

$$E_{Total}^{Required} = \int_{t_0}^{t_f} E_{Total}\, dt = W\left(\int_{t_0}^{t_f} h\, dt + \frac{1}{2g}\int_{t_0}^{t_f} V_a^2\, dt\right) \tag{7}$$

Furthermore the energy profile can be obtained through the acceleration profile, which can be analysed to its components, as illustrated in our earlier work (Kladis et al., 2008b). The components involve lateral and tangential acceleration. However, the latter depicts the *virtual* energy requirements for the UAV mission. According to the energy balance the rate of change of the aircraft energy (6) is equal to (8):

$$E_r = P_a - P_d + E_f \tag{8}$$

where P_a is the power available from fuel reserves on board, P_d is the dissipated power requirements by the overall opposing aerodynamic forces applied (i.e. drag D and wind profile F_w) and E_f the rate of energy change due to the change of weight of the aerial vehicle (i.e. for the case that it is fuel propelled). Hence, Eq. (8) expands to (9) by substituting (6):

$$\frac{P_a - F_{Total}V_a}{W} = \frac{dh}{dt} + \frac{V_a}{g}\frac{dV_a}{dt} = \frac{dE_s}{dt} \equiv P_s \tag{9}$$

The latter is termed specific excess power. All parameters considered previously are in *SI* units.

3. Tracking an error model under known weather conditions

As mentioned previously a crucial task for autonomous flying is tracking a predefined trajectory when wind disturbances are present. For tracking purposes, formulating the problem with respect to the error posture, rather than the inertial coordinates model of the vehicle, as illustrated previously, can aid the design of the control methodology. Particularly, the reference and the current posture are used for the generation of the error posture of the vehicle. Hence a set of reference postures denote a reference trajectory to be followed. Among the advantages of using such a model an important one is that there can be created any kind of reference trajectory to be tracked, even discontinuous ones.

In the included section the error posture model and the control methodology design to track a predefined trajectory are described. Additionally its equivalence is shown with respect to a Takagi–Sugeno (T–S) fuzzy model which is used in the control methodology. Moreover, the advantages of using a T–S model rather than the non-linear model are illustrated. The control methodology used involves a parallel distributed compensation (PDC) law to be computed via the use of linear matrix inequality (LMI) techniques.

3.1. Error posture model

In the error posture model the reference and the current posture used are denoted as $P_{ref}(X_{ref}, Y_{ref}, \theta_{ref})$ and $P_c(X_c, Y_c, \theta_c)$, respectively. The reference position is the position of vehicle to be tracked and the current is the *real* one calculated at each time step. The error model can be determined by applying a transformation of P_{ref} in the local frame with origin P_c and X-axis colinear with vector $\overrightarrow{\theta_c}$. The previous is illustrated in Fig. 1. Hence, the tracking error is governed by Eq. (10) as illustrated in Nelson (1988):

$$P_e = \mathbf{T}_e(P_{ref} - P_c) \tag{10}$$

where

$$\mathbf{T}_e = \begin{bmatrix} \cos(\theta_c) & \sin(\theta_c) & 0 \\ -\sin(\theta_c) & \cos(\theta_c) & 0 \\ 0 & 0 & 1 \end{bmatrix} \tag{11}$$

Hence instead of the direct kinematic model used in (1) with the necessary assumptions then the error posture model can be used for tracking purposes.

Proposition 1. *The error dynamics are equal to*

$$\dot{P}_e = \begin{bmatrix} \dot{x}_e \\ \dot{y}_e \\ \dot{\theta}_e \end{bmatrix} = \begin{bmatrix} y_e\omega_c - v_c + v_{ref}\cos(\theta_e) \\ -x_e\omega_c + v_{ref}\sin(\theta_e) \\ \dot{\theta}_{ref} - \dot{\theta}_c \end{bmatrix} = \begin{bmatrix} y_e\omega_c - v_c + v_{ref}\cos(\theta_e) \\ -x_e\omega_c + v_{ref}\sin(\theta_e) \\ \omega_{ref} - \omega_c \end{bmatrix} \tag{12}$$

Proof. Using Eq. (10) and $\dot{x}_{ref}\sin(\theta_r) = \dot{y}_{ref}\cos(\theta_r)$ for the kinematics model then

$$\begin{aligned}
\dot{x}_e &= (\dot{x}_{ref} - \dot{x}_c)\cos(\theta_c) + (\dot{y}_{ref} - \dot{y}_c)\sin(\theta_c) - (x_{ref} - x_c)\dot{\theta}_c\sin(\theta_c) \\
&\quad + (y_{ref} - y_c)\dot{\theta}_c\cos(\theta_c) \\
&= y_e\omega_c - v_c + \dot{x}_{ref}\cos(\theta_c) + \dot{y}_{ref}\sin(\theta_c) \\
&= y_e\omega_c - v_c + \dot{x}_{ref}\cos(\theta_{ref} - \theta_e) \\
&\quad + \dot{y}_{ref}\sin(\theta_{ref} - \theta_e) \\
&= y_e\omega_c - v_c + \dot{x}_{ref}[\cos(\theta_{ref})\cos(\theta_e) + \sin(\theta_{ref})\sin(\theta_e)] \\
&\quad + \dot{y}_{ref}[\sin(\theta_{ref})\cos(\theta_e) - \cos(\theta_{ref})\sin(\theta_e)] \\
&= y_e\omega_c - v_c + [\dot{x}_{ref}\cos(\theta_{ref}) + \dot{y}_{ref}\sin(\theta_{ref})]\cos(\theta_e) \\
&\quad + [\dot{x}_{ref}\sin(\theta_{ref}) - \dot{y}_{ref}\cos(\theta_{ref})]\sin(\theta_e) \\
&= y_e\omega_c - v_c + v_{ref}\cos(\theta_e)
\end{aligned}$$

In the same manner for the $\dot{y}_e$ it results

$$\begin{aligned}
\dot{y}_e &= -(\dot{x}_{ref} - \dot{x}_c)\sin(\theta_c) + (\dot{y}_{ref} - \dot{y}_c)\cos(\theta_c) - (x_{ref} - x_c)\dot{\theta}_c\cos(\theta_c) \\
&\quad - (y_{ref} - y_c)\dot{\theta}_c\sin(\theta_c) \\
&= -x_e\omega_c + \dot{x}_c\sin(\theta_c) - \dot{y}_c\cos(\theta_c) - \dot{x}_{ref}\sin(\theta_c) - \dot{y}_{ref}\cos(\theta_c) \\
&= -x_e\omega_c + \dot{x}_c\sin(\theta_{ref} - \theta_e) - \dot{y}_c\cos(\theta_{ref} - \theta_e) \\
&= -x_e\omega_c - \dot{x}_{ref}[\sin(\theta_{ref})\cos(\theta_e) - \cos(\theta_{ref})\sin(\theta_e)] \\
&\quad + \dot{y}_{ref}[\cos(\theta_{ref})\cos(\theta_e) + \sin(\theta_{ref})\sin(\theta_e)] \\
&= -x_e\omega_c + [\dot{x}_{ref}\cos(\theta_{ref}) + \dot{y}_{ref}\sin(\theta_{ref})]\sin(\theta_e) \\
&\quad + [\dot{y}_{ref}\cos(\theta_{ref}) - \dot{x}_{ref}\sin(\theta_{ref})]\cos(\theta_e) \\
&= -x_e\omega_c + v_{ref}\sin(\theta_e)
\end{aligned}$$

Lastly

$$\dot{\theta}_e = \dot{\theta}_{ref} - \dot{\theta}_c = \omega_{ref} - \omega_c$$

Hence Proposition 1 is proved. Eq. (12) can be reformulated as

$$\begin{bmatrix} \dot{x}_e \\ \dot{y}_e \\ \dot{\theta}_e \end{bmatrix} = \begin{bmatrix} \cos(\theta_e) & 0 \\ \sin(\theta_e) & 0 \\ 0 & 1 \end{bmatrix}\begin{bmatrix} v_{ref} \\ w_{ref} \end{bmatrix} + \begin{bmatrix} -1 & y_e \\ 0 & -x_e \\ 0 & -1 \end{bmatrix} u \tag{13}$$

where v_{ref} and w_{ref} are the linear and angular reference velocity, respectively. The control vector is $u^T = [v\ w]$. Klančar and Skrjanc (2007) have proposed a control law of $u = u_F + u_B$ where $u_F = [v_{ref}\cos(\theta_e) w_{ref}]^T$. u_F is a feed-forward control action vector whereas u_B a feedback control action vector. Hence substituting the previous to (13) expands to (14):

$$\begin{bmatrix} \dot{x}_e \\ \dot{y}_e \\ \dot{\theta}_e \end{bmatrix} = \begin{bmatrix} 0 & w_{ref} & 0 \\ -w_{ref} & 0 & v_{ref}\,\mathrm{sinc}(\theta_e) \\ 0 & 0 & 0 \end{bmatrix}\begin{bmatrix} x_e \\ y_e \\ \theta_e \end{bmatrix} + \begin{bmatrix} -1 & y_e \\ 0 & -x_e \\ 0 & -1 \end{bmatrix} u_B \tag{14}$$

The reference linear velocity v_{ref} and angular velocity w_{ref} can be computed using Eqs. (15) and (16), respectively:

$$v_{ref} = \sqrt{\dot{x}_{ref}^2 + \dot{y}_{ref}^2} \tag{15}$$

$$w_{ref} = \frac{\dot{x}_{ref}\ddot{y}_{ref} - \dot{y}_{ref}\ddot{x}_{ref}}{\dot{x}_{ref}^2 + \dot{y}_{ref}^2} \tag{16}$$

where $\dot{k}$, $\ddot{k}$ denote the first and second derivatives, respectively, with time. u_B is calculated in the analysis by the use of a PDC (parallel distributed compensation) control law. The control law used is designed to guarantee stability within a compact region of space and the gains are calculated through the use of LMI (linear matrix inequality) conditions. The latter is illustrated in Section 3.3.

3.2. Equivalence of error posture model with the Takagi–Sugeno model

Fuzzy logic control was originally introduced to describe complicated nonlinear systems where knowing the actual physical phenomena was not a prerequisite for their development. Hence, it is a model free control design approach. Although its has been successfully applied to numerous industrial control problems a systematic analysis for proving stability of the system is still a challenging task. Thus research turned towards model-based systems like the Takagi–Sugeno (T–S) fuzzy model (Takagi and Sugeno, 1985), also referred to as the Type-III fuzzy model. The T–S is a combination of linear models that can represent satisfactorily a nonlinear model with a compromise of complexity and error. The latter method produces an alternative approach to describing complex nonlinear systems and is described in this section. The T–S model can be described through the following polytopic form as suggested in Sugeno and Kang (1986):

$$\dot{X}(t) = \sum_{i=1}^{r} \lambda_i(z(t))[\mathbf{A}_i\mathbf{X}(t) + \mathbf{B}_i\mathbf{U}_\mathbf{b}(t)]$$

$$Y(t) = \sum_{i=1}^{r} \lambda_i(z(t))\mathbf{C}_i\mathbf{X}(t) \tag{17}$$

$X(t)$, $Y(t)$ are the state and output vectors, $z(t)=[z_1(t),z_2(t),\ldots,z_p(t)]^T$ the premise vector which may depend on the state vector and A_i,B_i,C_i are constant matrices. The rules are denoted with r and their number is equal to $2^{|z|}$, where notation $|z|$ denotes the number of nonlinearities considered. The latter clearly depicts its dependency to the *premise* variables $z_i(t)$ considered in the system. In addition λ_i are normalised weighted functions which are defined by

$$\lambda_i(z(t)) = \frac{w_i(z(t))}{\sum_{i=1}^{r} w_i(z(t))}$$

$$w_i(z(t)) = \prod_{j=1}^{p} M_{ij}(z_j(t)) \tag{18}$$

$M_{ij}(z_j(t)) \in [0,1]$ denotes the ranking of the membership function of the premise variable $z_j(t)$ in M_{ij} and $\lambda_i(z(t))$ satisfies the convex sum property for all t. The nonlinear system is modelled as a T–S model in a compact region of the state space variable using the sector nonlinearity approach (Kawamoto et al., 1992). This approach guarantees an exact approximation, however, it is often difficult to find global sectors for general nonlinear systems. Thus local sectors are utilised since variables in nonlinear systems can be bounded. The latter means that every bounded nonlinear term (premise variable) is decomposed in a convex combination of its bounds as suggested in Sugeno and Kang (1986). In essence the compact region for the premise variables should be known a priori in order for the previous to hold. Additionally the membership functions used in this work are triangular types. Note that the fuzzy model is an approximated model. On the other hand, if an exact approximation is needed then more complicated membership functions need to be considered as suggested in Tanaka and Wang (2001).

There are four important steps involved in order to develop the equivalent T–S fuzzy model to the nonlinear system. Those are:

- Definition of the premise variables of the nonlinear system and calculation of their compact region.
- Definition of the membership functions.
- Determination of the number of rules involved and each rule with respect to possible associations between the premise variables.
- Calculation of A_i,B_i and C_i with respect to the compact region of the premise variables.

The latter steps are thoroughly described in the simulation example illustrated in this work.

3.3. Stabilising the Takagi–Sugeno model

As mentioned previously, the fuzzy controller used for the T–S Fuzzy system is the so-called parallel distributed compensation (PDC) proposed by Sugeno and Kang (1986) and later improved in Wang et al. (1995). In the PDC design every control law to be used, 16 in total for the aircraft model illustrated, is designed from the rules of the T–S fuzzy model, respectively. In other words, it involves the same fuzzy sets in the premise part with the T–S model fed. Hence for the fuzzy model described by Eq. (17) the ith control rule layout is equivalent to the following:

Rule i: **IF** $z_1(t)$ is M_{i1} **AND** ... **AND** $z_p(t)$ is M_{ip} **THEN** $\mathbf{U_b}(t) = -\mathbf{F_i}X(t)$ for $i=1,2,\ldots,r$ where $p=|z|$. Thus the layout falls under category of state feedback laws. The overall state feedback law to be used in the design has the form of

$$\mathbf{U}_b(t) = -\frac{\sum_{i=1}^{r} w_i(z(t))\mathbf{F}_i X(t)}{\sum_{i=1}^{r} w_i(z(t))} = -\sum_{i=1}^{r} \lambda_i(z(t))\mathbf{F}_i X(t) \tag{19}$$

The matrices $\mathbf{F}_i$ are the local feedback gains that are calculated in order to guarantee global stability of the system. The latter is performed through the use of LMI (linear matrix inequality) conditions which can guarantee global stability in the consequent compact regions of the premise parts. Since the latter aspect is beyond the scope of this work only the conditions involved in the included analysis are discussed in brevity. For a thorough treatment of the subject of stability with LMI conditions, designs, convergence, proofs, etc. the interested reader may refer to Tanaka and Wang (2001). The conditions used for the LMI are the ones proposed by work (Tanaka and Wang, 2001) which suggested that the TS model can be stabilised via PDC control law, a decay rate, constraint on control input and one for disturbance rejection.

Theorem 1 (*Tanaka and Wang, 2001*). *The T–S model* (17) *can be stabilised via the PDC control law* (19) *if it exists symmetric positive matrix* $X>0$ *and matrices* M_i *with* $i \in 1,2,\ldots,r$ *such that the following conditions* (20) *hold*:

$$\begin{cases} \Upsilon_{ii} < 0, \quad i \in \{1,2,\ldots,r\} \\ \Upsilon_{ij} + \Upsilon_{ji} < 0, \quad i,j \in \{1,2,\ldots,r\}, \quad i<j \text{ s.t. } \lambda_i \cap \lambda_j \neq \emptyset \end{cases} \tag{20}$$

where $\Upsilon_{ij} = \mathbf{X}\mathbf{A}_i^T + \mathbf{A}_i\mathbf{X} - \mathbf{B}_i\mathbf{M}_j - \mathbf{M}_j^T\mathbf{B}_i^T$. *Moreover, if the conditions hold, the PDC control law gains are given by*

$$\mathbf{F}_i = \mathbf{M}_i\mathbf{X}^{-1} \tag{21}$$

Remark. The conditions are only sufficient; many works in the literature try to lower the pessimism of these conditions. Two ways are investigated, using some properties of the $\lambda_i(z(t))$ functions

(Sala and Ariño, 2007; Tuan et al., 2001) or some slack variables (Liu and Zhang, 2003). The first one has been *closed* in a way in Sala and Ariño (2007) using the Polya's approach. Without adding the slack variables, Theorem 2 conditions lead to a good compromise between complexity and conservatism.

Theorem 2 (*Tuan et al., 2001*). *With the* Υ_{ij} *defined previously, the stabilisation of the T–S model* (17) *is ensured if the following conditions* (22) *hold*:

$$\begin{cases} \Upsilon_{ii} < 0, \quad i \in \{1,2,\ldots,r\} \\ \dfrac{2}{r-1}\Upsilon_{ii} + \Upsilon_{ij} + \Upsilon_{ji} < 0, \quad i,j \in \{1,2,\ldots,r\}, \quad i \neq j \ s.t. \ \lambda_i \cap \lambda_j \neq \emptyset \end{cases} \tag{22}$$

In order to include some performances in the conditions, several approaches are possible. A decay rate α *can be introduced, i.e. considering the Lyapunov function*: $\dot{V}(x) + 2\alpha V(x) < 0$. *Therefore just replace the previous* Υ_{ij} *with* : $\Upsilon_{ij} = \mathbf{X}\mathbf{A}_i^T + \mathbf{A}_i\mathbf{X} - \mathbf{B}_i\mathbf{M}_j - \mathbf{M}_j^T\mathbf{B}_i^T + 2\alpha\mathbf{X}$ *and use a generalised eigenvalue problem* (Boyd et al., 1994):

$$\underset{\mathbf{X},\mathbf{M}_1,\ldots,\mathbf{M}_r}{\text{maximise}} \ \alpha \tag{23}$$

$$\begin{cases} \mathbf{X} > 0 \\ \Upsilon_{ii} < 0, \quad \in \{1,2,\ldots,r\} \\ \dfrac{2}{r-1}\Upsilon_{ii} + \Upsilon_{ij} + \Upsilon_{ji} < 0, \quad i,j \in \{1,2,\ldots,r\}, \quad i \neq j \ s.t. \lambda_i \cap \lambda_j \neq \emptyset \end{cases} \tag{24}$$

Provided that initial conditions are a priori known through a particular strategy then a constraint on the input of $\|u\|_2 \leq \mu$ *can also be enforced, throughout the time horizon, subject to constraints* (25) *and* (26) *as suggested in* Boyd et al. (1994):

$$\begin{bmatrix} 1 & x(0)^T \\ x(0) & \mathbf{X} \end{bmatrix} \geq 0 \tag{25}$$

$$\begin{bmatrix} \mathbf{X} & \mathbf{M}_i^T \\ \mathbf{M}_i & \mu^2\mathbf{I} \end{bmatrix} \geq 0 \tag{26}$$

Moreover, in order to accommodate more closely real world conditions disturbances while in flight can be present. For instance the presence of winds cannot be neglected from the aerodynamic frame while in flight. Hence it should be accounted in the design and control actions should be applied in order to track a predefined type of trajectory. Hence the T–S model (17) *becomes*

$$\dot{X}(t) = \sum_{i=1}^{r} \lambda_i(z(t))[\mathbf{A}_i\mathbf{X}(t) + \mathbf{B}_i\mathbf{U}_b(t) + \mathbf{E}_i\upsilon(t)]$$

$$Y(t) = \sum_{i=1}^{r} \lambda_i(z(t))\mathbf{C}_i\mathbf{X}(t) \tag{27}$$

where the components $\mathbf{E}_i\upsilon(t)$ *denote the disturbance taken into account. Hence the problem results to the one minimising* γ *subject to*

$$\sup_{\|\upsilon(t)\|_2 \neq 0} \frac{\|y(t)\|_2}{\|\upsilon(t)\|_2} \leq \gamma \tag{28}$$

Hence minimise γ *subject to*

$$\underset{\mathbf{X},\mathbf{M}_1,\ldots,\mathbf{M}_r}{\text{minimise}} \ \gamma^2 \tag{29}$$

$$\begin{cases} \Upsilon_{ii} < 0, \quad i \in \{1,2,\ldots,r\} \\ \dfrac{2}{r-1}\Upsilon_{ii} + \Upsilon_{ij} + \Upsilon_{ji} < 0, \quad i,j \in \{1,2,\ldots,r\}, \quad i \neq j \ s.t. \ \lambda_i \cap \lambda_j \neq \emptyset \end{cases} \tag{30}$$

where Υ_{ij} *is equal to*

$$\Upsilon_{ij} = \begin{bmatrix} \mathbf{X}\mathbf{A}_i^T + \mathbf{A}_i\mathbf{X} - \mathbf{B}_i\mathbf{M}_j - \mathbf{M}_j^T\mathbf{B}_i^T & -\mathbf{E}_i & \mathbf{X}\mathbf{C}_i^T \\ -\mathbf{E}_i^T & -2\gamma^2\mathbf{I} & 0 \\ \mathbf{C}_i\mathbf{X} & 0 & -2\mathbf{I} \end{bmatrix} \tag{31}$$

It should be mentioned that relaxed LMI conditions exist. The latter can prove helpful because there is an increase of the degrees of freedom of finding a common $\mathbf{X}$ *in a largest compact space. In other words, if the number of rules is a large number then it might be difficult to find a common* $\mathbf{X}$ *satisfying the conditions mentioned. Thus relaxed stability conditions can be helpful towards proving global stability for the system. Among many interesting works, to name a few* Guerra and Vermeiren (2004), Guerra et al. (2006), Khiar et al. (2007), Bernal et al. (2009) *deal with the latter aspects. The conditions illustrated in this section are used in the simulation example.*

4. Simulation example

In this section the methodology described previously is going to be illustrated through a simulation example. For the scenario illustrated the wind profile is a priori known and the task is for a UAV to find the shortest route with respect to energy requirements in order to travel from a priori known location to a destination. Additional tasks require the UAV to track the predefined reference path, reject wind disturbances while fulfilling mission requirements. For the purpose of illustration the example is divided into three different subsections and is mostly involved with the preflight planning phase. By the former the assumptions for the scenario are outlined. Thereafter, the routing problem is addressed and described. Lastly, the generation of the energy cost matrix $\mathbf{P}$ and the tracking problem are described.

4.1. Assumptions

For the scenario illustrated it is assumed that ground speed and altitude can be maintained constant provided that control surfaces are robust. By maintaining constant ground velocity it implies that time to reach a destination (i.e. for traffic purposes) can be estimated provided that the UAV can afford the adequate propulsive means to overcome disturbances. Additionally, it can be used in scenarios of simultaneous rendezvous of a group of UAVs. When under wind disturbances, in order to regulate ground velocity the propulsive forces are varying. For instance, for a tailwind the magnitude of the thrust force is decreasing and the specific energy is decreasing. Corollary, the power demand is decreasing. In essence there is saving in power (fuel consumed). On the other hand, for a head wind, propulsive forces are increased to maintain ground speed and the power demand is increasing. The previous can occur provided $|V_w| \ll |V_g|$ and there are enough propulsive resources to overcome a disturbance.

Maintaining constant altitude can be assumed under realistic scenarios where the operational regime requires for the UAV to fly at a particular altitude within which there are no conflicting paths with flight traffic. Also due to particular atmospheric properties a particular altitude can be fuel saving. Additionally, it can be assumed due to mission constraints (i.e. on reconnaissance missions the UAV needs to photograph a region in a stealthy manner). The operational altitude assumed for the scenarios illustrated further on is 1 km above sea level.

The source and the destination node for the UAV to start and finish its mission are a priori known. Moreover the number of nodes involved in the graph G (representation of map) are 100. The graph considered is a sparse one and there is also overlapping between edges connecting adjacent nodes. Each node considered is a topological section rather than a point with particular coordinates within the map.

The calculation of gains for the tracking module is performed at the preflight planning phase. Hence performance is guaranteed in

real-time. In essence there are no delays in computations carried out while on flight.

Furthermore prior knowledge is assumed with respect to properties of the wind profile due to Doppler weather radars or anemometers placed at masts over buildings (when flying at low altitude). The wind profile has magnitude and direction in global frame. It is assumed that the wind profile is varied in an incipient manner through out the entire map. In addition $|V_w| \ll |V_g|$.

The standard type of path to be followed, under specific minimum turning radius, is a Dubins path mentioned in Section 2.3. Particularly, the minimum turning radius in our case is 40 m. Moreover every node is constrained to a particular heading angle which is assumed a priori. The previous realistic assumption can accommodate scenarios of surveillance where the UAV is equipped with a camera sensor with a mission to photograph particular sections of the map. Hence in order to fulfil the mission objectives the UAV is needed to approach the particular pose with a particular heading angle.

4.2. The routing problem

The routing problem illustrated in this section, that is to say for the UAV to travel from a source node to a destination with the minimum energy demand falls under category of shortest path problems. Due to the problem requirements and application domain shortest path algorithms are utilised for its solution. For a thorough treatment of the adequate choice of the shortest path algorithm to be used the interested reader may refer to Kladis (2010). For the simulation example illustrated the Dijkstra (1959) algorithm is used. The task described herein is for:

An UAV is deployed in a priori known map, represented by a graph G(V,E), under known environmental conditions. Determine the optimum route in a safe-flyable energy efficient manner while starting and finishing at a priori known locations and satisfying heterogenous functional/physical constraints of the aerial vehicle.

Mathematically, provided that the map is described by a graph G then the graph can be represented by its unique adjacency matrix $\mathbf{P}[w_{[ij]}]$. Its generation is described in the next section. Each element w_{ij} depicts the energy requirements to travel from node i to j. Hence the task is to find the optimum sequence of nodes that yields the minimum total value of cost function (32), while satisfying the source and terminal constraints (starting and destination nodes). The objective function is equal to

$$COST_{path} = \sum_{i=1}^{n}\sum_{j=1}^{n} w_{ij}x_{ij} \tag{32}$$

subject to

$$w_{ii} = \infty, \quad \forall i \in V \tag{33}$$

$$\sum_{j} x_{ij} - \sum_{j} x_{ji} = m, \quad \forall i,j \in V \tag{34}$$

where

$$m = \begin{cases} 0 & \text{otherwise} \\ 1 & \text{for } i = t \\ -1 & \text{for } i = s \end{cases} \tag{35}$$

where term $x_{ij} \in \{0,1\}$ $\forall i,j \in V$ represents a decision variable that denotes whether or not the particular walk is considered. Additionally s and t coincide with the source and destination nodes. Thus the second constraint impose the referred "flow-conservation". Furthermore the diagonal elements of the energy cost matrix are set to infinity (first constraint) in order to guarantee that there are no cyclic modes in the graph. In other words for the vehicle not to stay in a particular node, contrary use it as an intermediate node to traverse the map.

Hence, following the block diagram depicted in Fig. 3, firstly a map is represented by a graph $G(V,E)$ as illustrated in Fig. 5. The source and destination nodes are 90 and 54 , respectively. Utilising the reachability property, addressed in work (Economou et al., 2007b), it can be

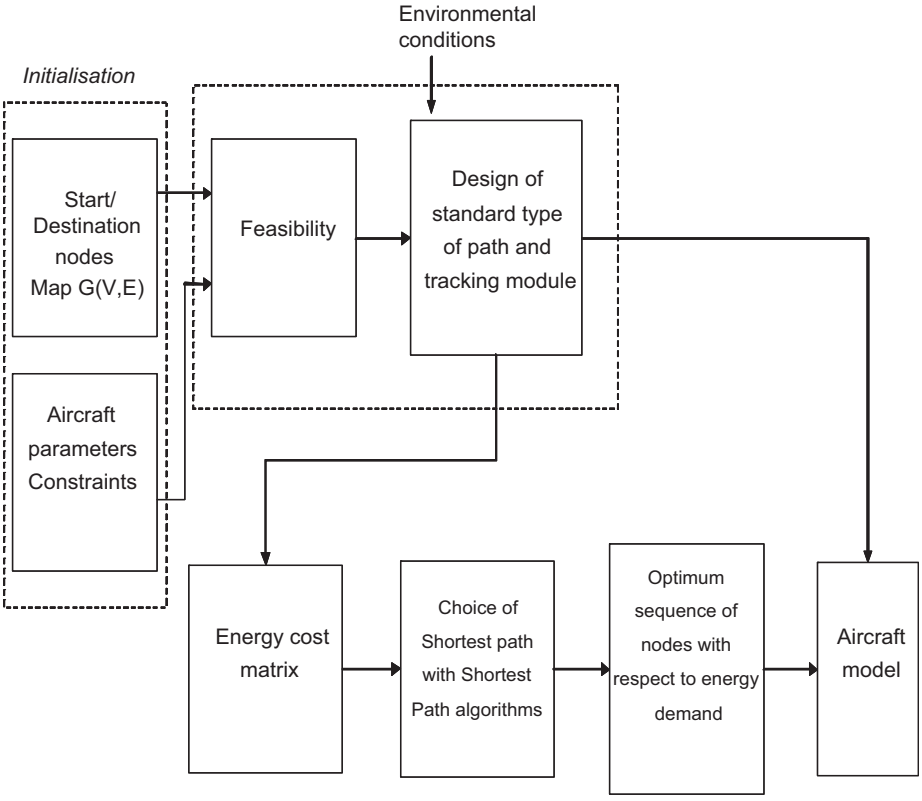

Fig. 3. Block diagram of the total procedure.

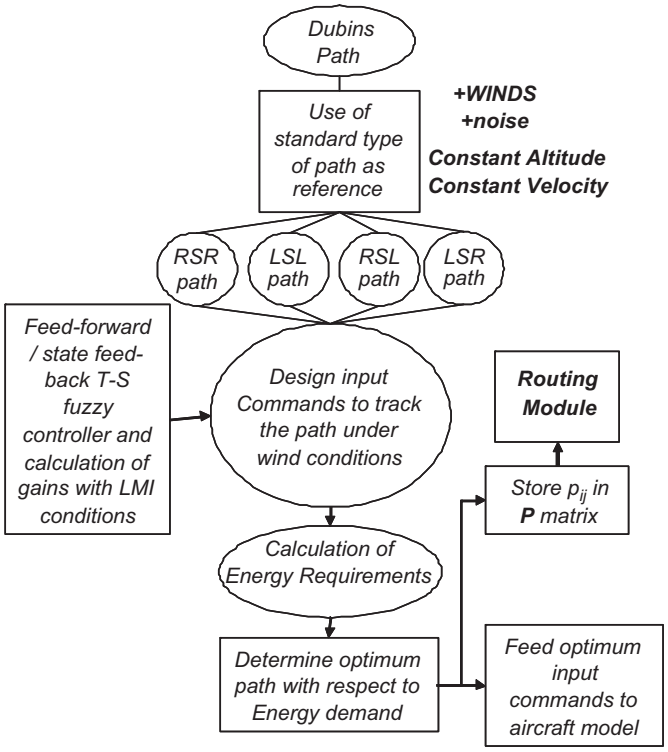

Fig. 4. Block diagram of the generation of the energy cost matrix for the node to node walk.

easily be determined whether the mission is feasible or not. Thereafter the four different Dubins paths $s_i(t)$ are designed through the use of Euclidean principles as suggested in Shanmugavel (2007). The number of the different Dubins paths is due to the heading constraints for each node to node sequence. Those trajectories are fed in to the aircraft model which is under unknown wind profile. The task involved at this stage is dual. Firstly the adequate input commands need to be determined in order to track $s_i(t)$ and then calculation of the energy profile is also required. Both steps are performed as illustrated in Sections 3 and 2.5. Thereafter from Eq. (7) the set of total energy demands $P=p^i, i=1,\ldots,4$ to follow the paths $s_i(t)$, respectively, are stored and the minimum p_i is assigned to the *Energy Demand matrix* **P** which is illustrated in Fig. 8. Additionally the adjacency matrix for the Euclidean distance and connectivity coincide with Figs. 7 and 6, respectively. The profile of the magnitude of wind with respect to its localisation a priori assumed is depicted by the contours in Fig. 5. The direction of the wind with respect to the global frame is denoted by the black solid arrows in Fig. 5. For simplicity it is assumed that the magnitude is varied in an incipient manner as mentioned in Section 2.4, whereas the direction is constant through the entire walk $i \rightarrow j$. Thereafter the Dijkstra algorithm is utilised and the classic shortest path problem is solved. In essence, cost function (32) is minimised subject to constraints. The optimum path with respect to energy requirements and the total cost for the UAV to start from the source and finish at the destination node are returned. The route of minimum total energy requirements is the sequence {90,82,36,80,75,60,98,35 *and* 54}. The optimum route is depicted in dotted solid red in Fig. 5. The total cost is 489 340 J s. For the interested reader the thesis by Kladis (2010) illustrated the energy requirements

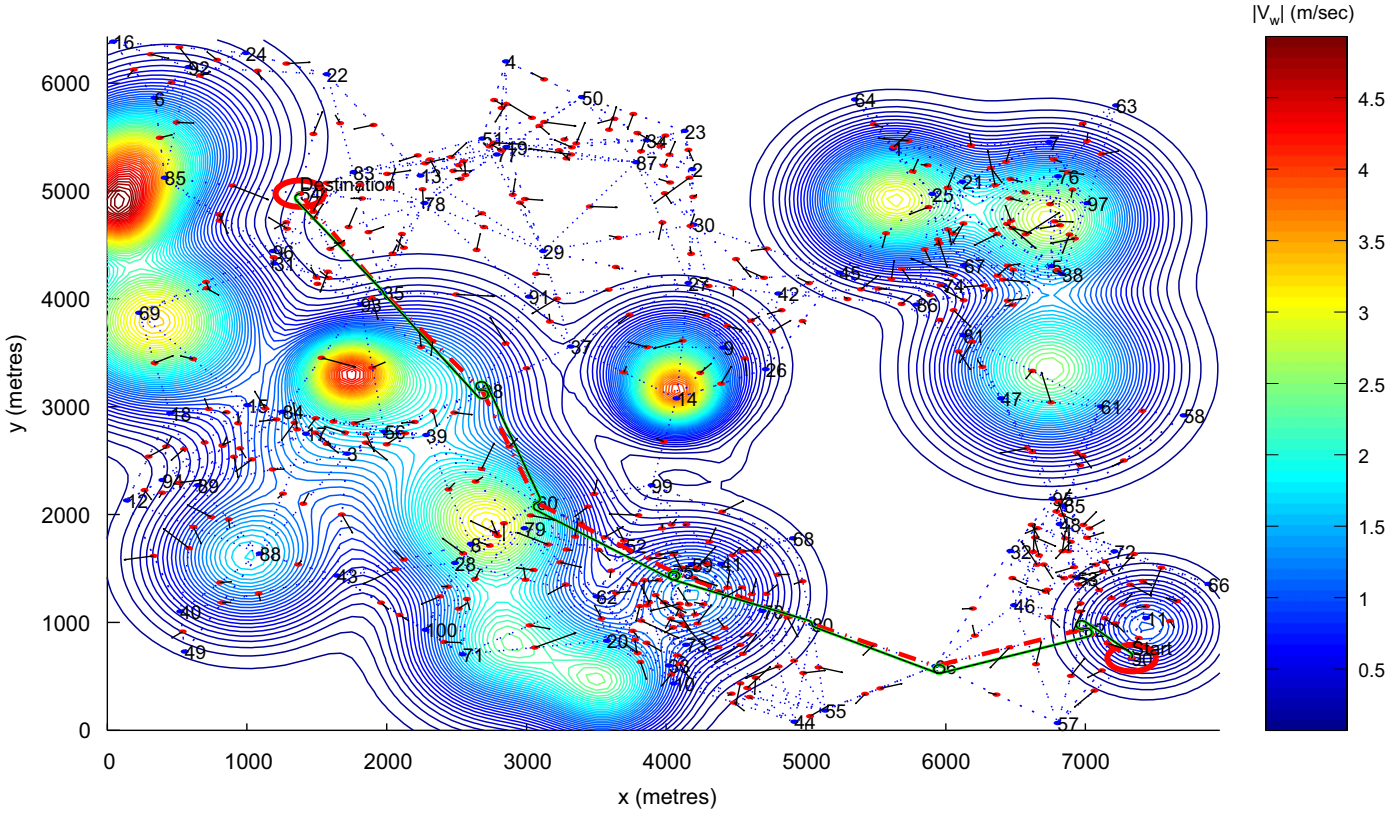

Fig. 5. Representation of mission, optimum energy path (in red) under wind conditions in the global frame and Dubins trajectories for nominal (in solid green) and tracked path (in black). Red circles depict the source and the destination nodes. Arrows coincide with the direction of wind profile in the global frame. Contours depict the magnitude of wind with respect to localisation. Optimum energy route returned from the Dijkstra algorithm in dotted red. (For interpretation of the references to colour in this figure legend, the reader is referred to the web version of this article.)

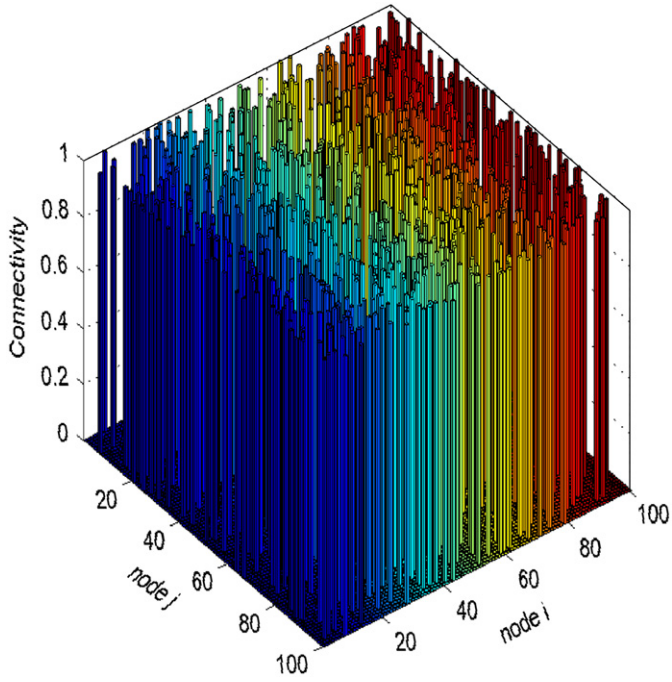

Fig. 6. Adjacency matrix representing connectivity for the node to node paths in the Graph.

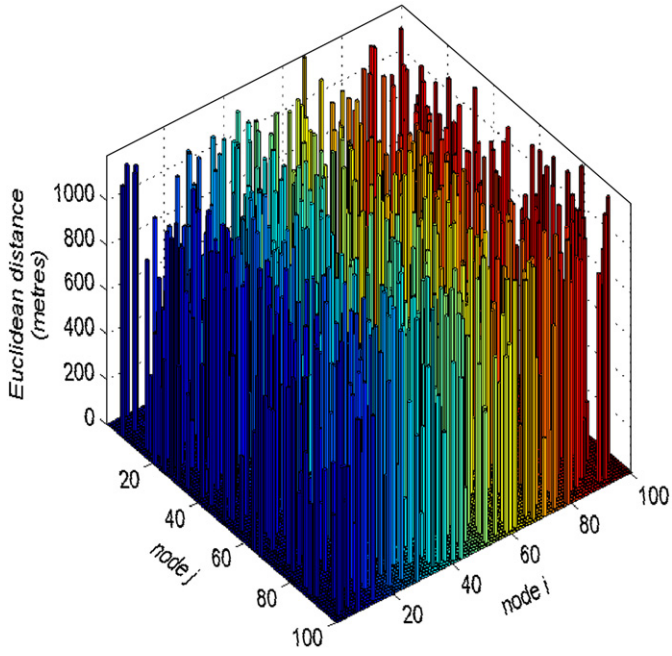

Fig. 7. Adjacency matrix representing Euclidean distance for the node to node paths in the graph.

saved for a UAV mission when choosing a longer path (with wind-favourable walks) rather than the shortest Euclidean path.

4.3. Generation of the energy cost matrix and the tracking problem

In the included section the generation of the **P** adjacency matrix used earlier is described. The generation of the **P** adjacency matrix involve for the preflight planning to update the energy demand needed for the UAV to travel from nodes i to j, for every possible node to node path. The entire procedure for the generation of **P** is illustrated in Fig. 4.

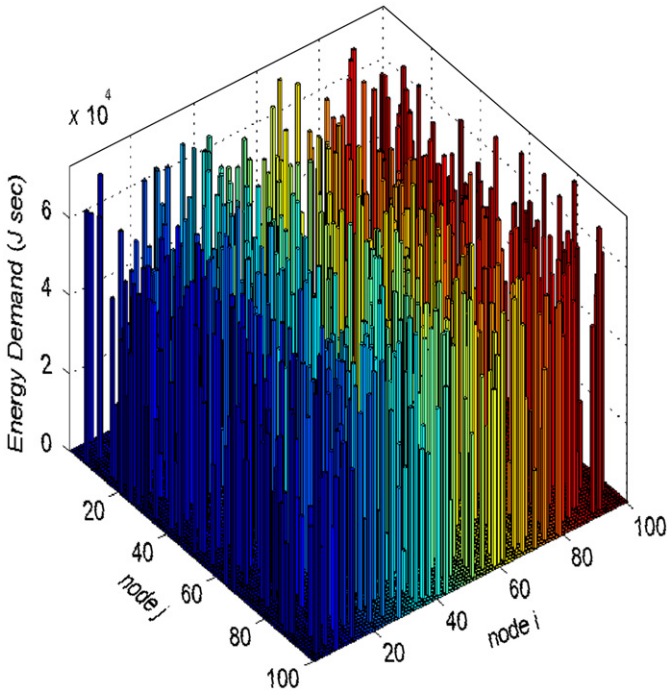

Fig. 8. Total energy demand adjacency matrix.

Following block diagram in Fig. 4, for two adjacent nodes P_i and P_j with particular poses $P_i(x_i,y_i,\theta_i)$ and $P_j(x_j,y_j,\theta_j)$ there are four different trajectories connecting those. In the problem illustrated the lowest-energy-required path is chosen when under wind conditions. Hence for each node to node sequence the lowest-energy-required path is stored in adjacency matrix $\mathbf{P}=[\min(p^*_{ij})]$. The latter is fed to the routing module in order to determine the shortest path. For instance let us assume that the poses are the ones depicted in Fig. 9 and the four alternative Dubins paths, RSR, LSL, RSL and LSR are the ones depicted in Fig. 9 (top). The energy demand to track the predetermined paths s_o, under the same weather conditions, are the ones depicted in Fig. 9 (bottom). The energy demand is calculated as suggested in Section 2.5. For the previous example the operational altitude is 10 m above sea level. Hence the energy demand that is chosen to be stored in **P** coincides with the RSL trajectory. The above procedure is repeated until every element in matrix **P** is updated. The procedure involved for its update is illustrated further on.

The T–S fuzzy model is derived following the four steps mentioned in Section 3.2. For the model illustrated in Eq. (14) the premise variables determined are four. Those are $z_1=w_{ref}$, $z_2=V_{ref}\mathrm{sinc}(\theta_e)$, $z_3=x_e$ and $z_4=y_e$. In addition the rules of the fuzzy system are $r=16$. Moreover for variables V_{ref}, w_{ref}, x_e, y_e and θ_e the compact region for the premise variables is calculated. Hence $z_1\in[a_1^{min}a_1^{max}]=[-0.513,0.513]$, $z_2\in[a_2^{min}a_2^{max}]=[18.0048,20]$, $z_3\in[a_3^{min}a_3^{max}]=[-1.5,1.5]$ and $z_4\in[a_4^{min}a_4^{max}]=[-1.5,1.5]$. In addition $\theta_e\in[-\pi/4,\pi/4]$. It should be noted that the latter bounds are not chosen in an arbitrary manner, however, those are assumed in order not to lose controllability of the system. Thereafter at the second step:

$$z_j(t)=O_0(z_j(t))a_j^{\min}+O_1(z_j(t))a_j^{\max},\quad \forall O\in\{M,N,\Xi,\Theta\}\quad\text{and}\quad \forall j\in\{1,2,3,4\} \tag{36}$$

Additionally all the ranking functions $O\in\{M,N,\Xi,\Theta\}$ suffice

$$\sum_i^k O_i(z_j(t))=1,\quad \forall k\in\{0,1\} \tag{37}$$

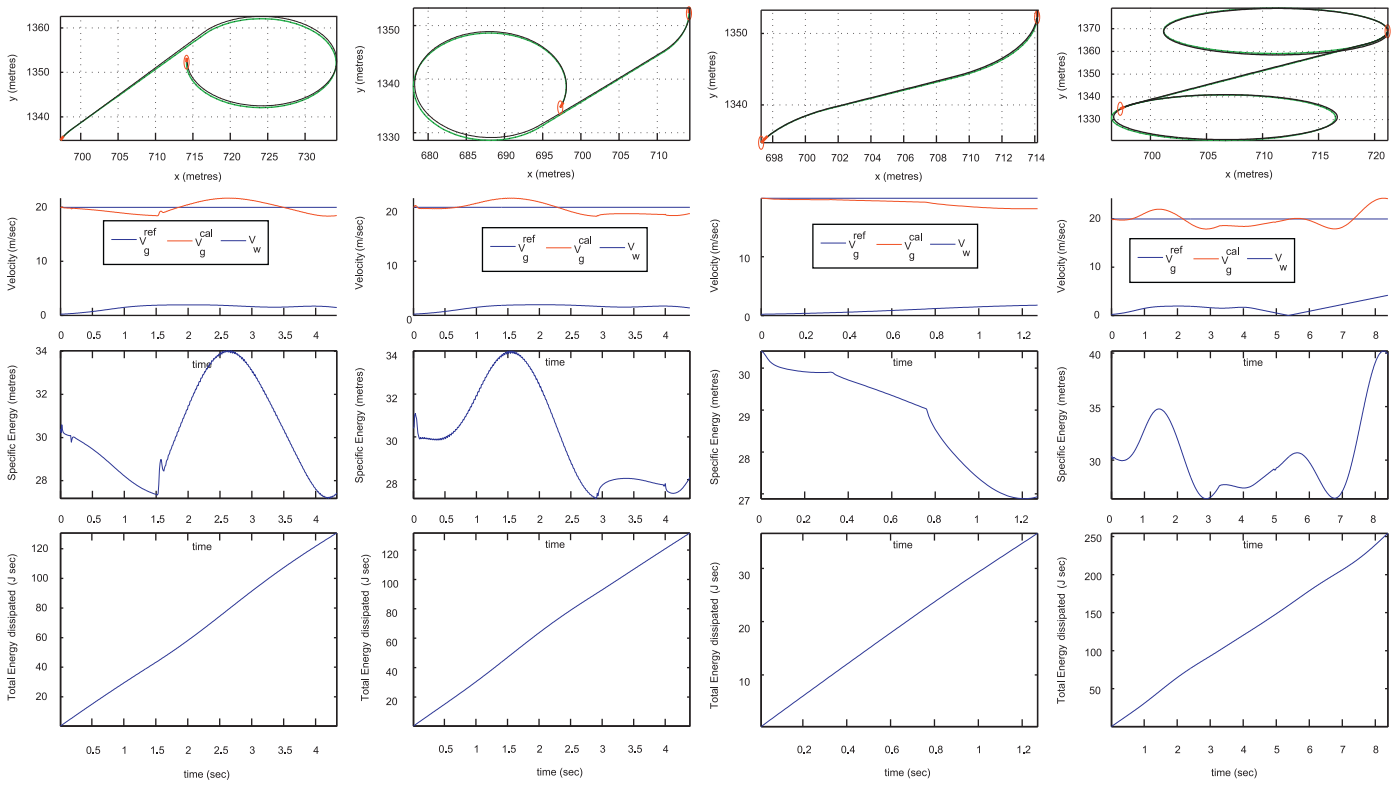

Fig. 9. Example trajectories for a node to node path and selection of the less energy-demanding route for s_i trajectories (RSR, LSL, RSL and LSR). From top to bottom: trajectory taken into account; velocity profile (magnitude of reference ground speed, calculated one and magnitude of wind speed involved in the path); specific energy; and total energy demand for the path. RSL path is the optimum due to the total energy requirement.

Hence from Eqs. (36) and (37) the membership functions are calculated. The membership functions that depend on the premise variables z_1, z_2, z_3 and z_4, are depicted in Fig. 10, respectively. Thereafter all the possible sixteen rules are developed in the following manner:

Model Rule i: **IF** $z_1(t)$ is M_{ij} **AND** $z_2(t)$ is N_{ij} **AND** $z_3(t)$ is Ξ_{ij} **AND** $z_4(t)$ is Θ_{ij} **THEN** $\dot{X}(t)=\mathbf{A}_i\mathbf{X}(t)+\mathbf{B}_i\mathbf{U_b}(t)$.

Furthermore $\mathbf{A}_i$, $\mathbf{B}_i$ and $\mathbf{C}_i$ can be computed through the following recursive procedure:

Step (a) $i\leftarrow 1$;
Step (b) Assign $a_1=a_1^{min}{:}a_1^{max}-a_1^{min}{:}a_1^{max}$.
Step (c) Assign $a_2=a_2^{min}{:}a_2^{max}-a_2^{min}{:}a_2^{max}$.
Step (d) Assign $a_3=a_3^{min}{:}a_3^{max}-a_3^{min}{:}a_3^{max}$.
Step (e) Assign $a_4=a_4^{min}{:}a_4^{max}-a_4^{min}{:}a_4^{max}$.
Step (f)
$$A_i=\begin{bmatrix}0 & a_1 & 0\\ -a_1 & 0 & a_2\\ 0 & 0 & 0\end{bmatrix} \quad \text{and} \quad B_i=\begin{bmatrix}-1 & a_3\\ 0 & -a_4\\ 0 & -1\end{bmatrix}$$
Step (g) Let $i\leftarrow i+1$ and go to step (b).

The state $\mathbf{A}_i$, input $\mathbf{B}_i$ and output matrices $\mathbf{C}_i$ can be found in the Appendix. The defuzzification is carried out with respect to Eq. (17), where λ_i are equal to

$$\lambda_{\overline{i\ell m\omega}}(z(t))=M_i(z_1)\times N_\ell(z_2)\times \Xi_m(z_3)\Theta_\omega(z_4), \quad \forall i,\ell,m,\omega\in\{0,1\} \tag{38}$$

with $(\overline{i\ell m\omega})_2=i\times 2^3+\ell\times 2^2+m\times 2^1+\omega\times 2^0+1$. $\underline{f}_j^T\le[f_j]^T\le\overline{f}_j^T$, $\underline{f}_j$ and $\overline{f}_j$ are the minimum and maximum values, respectively, for the premise variables. Hence, verifying the convex sum property, the ranking functions O are equal to

$$O_1(z_j(t))=\frac{\overline{f}_j-f_j}{\overline{f}_j-\underline{f}_j} \quad \text{and} \quad O_2(z_j(t))=1-O_1(z_j(t)) \tag{39}$$

The second term (i.e. O_2) is guaranteeing that the alpha cuts in the membership functions are in 50%. The previous procedure is representing the nonlinear system within the compact space of x_e, y_e and θ_e.

Hence the equivalent T–S fuzzy model (17) to the full nonlinear one (14) is derived. For model (17):

$$A_i=\begin{bmatrix}0 & -\varepsilon_i^1 w_{r,max} & 0\\ \varepsilon_i^1 w_{r,max} & 0 & \mu_i\\ 0 & 0 & 0\end{bmatrix} \quad \text{and} \quad B_i=\begin{bmatrix}-1 & \varepsilon_i^3 e_{max}\\ 0 & \varepsilon_i^4 e_{max}\\ 0 & -1\end{bmatrix},$$

$w_{r,\max}=0.513$ rad/s, $e_{max}=1.5$ m and

$$\varepsilon_i^1=\begin{cases}-1 & \text{for } 1\le i\le 8\\ +1 & \text{otherwise}\end{cases} \tag{40}$$

$$\mu_i^1=\begin{cases}18.0048 & \text{for } 1\le i\le 4 \quad \text{and} \quad 9\le i\le 12\\ 20 & \text{otherwise}\end{cases} \tag{41}$$

$$\varepsilon_i^3=\begin{cases}+1 & \text{otherwise}\\ -1 & \text{for } i\in\{1,2,5,6,9,10,13,14\}\end{cases} \tag{42}$$

$$\varepsilon_i^4=(-1)^{i+1} \tag{43}$$

The model is stabilised with the use of the PDC control law of the form of (19). The gains are calculated using the three different conditions as illustrated in Section 3.3. By the former a decay rate, an input compensation and finally a disturbance rejection condition are included. The F_i gains calculated can be found in the Appendix. Hence let us assume that the predefined path to be tracked is the one illustrated in green in Fig. 5. The reference trajectory to be tracked is the Dubins path.

In addition, the aerial vehicle is flying under a priori known weather conditions with magnitude and direction with respect to

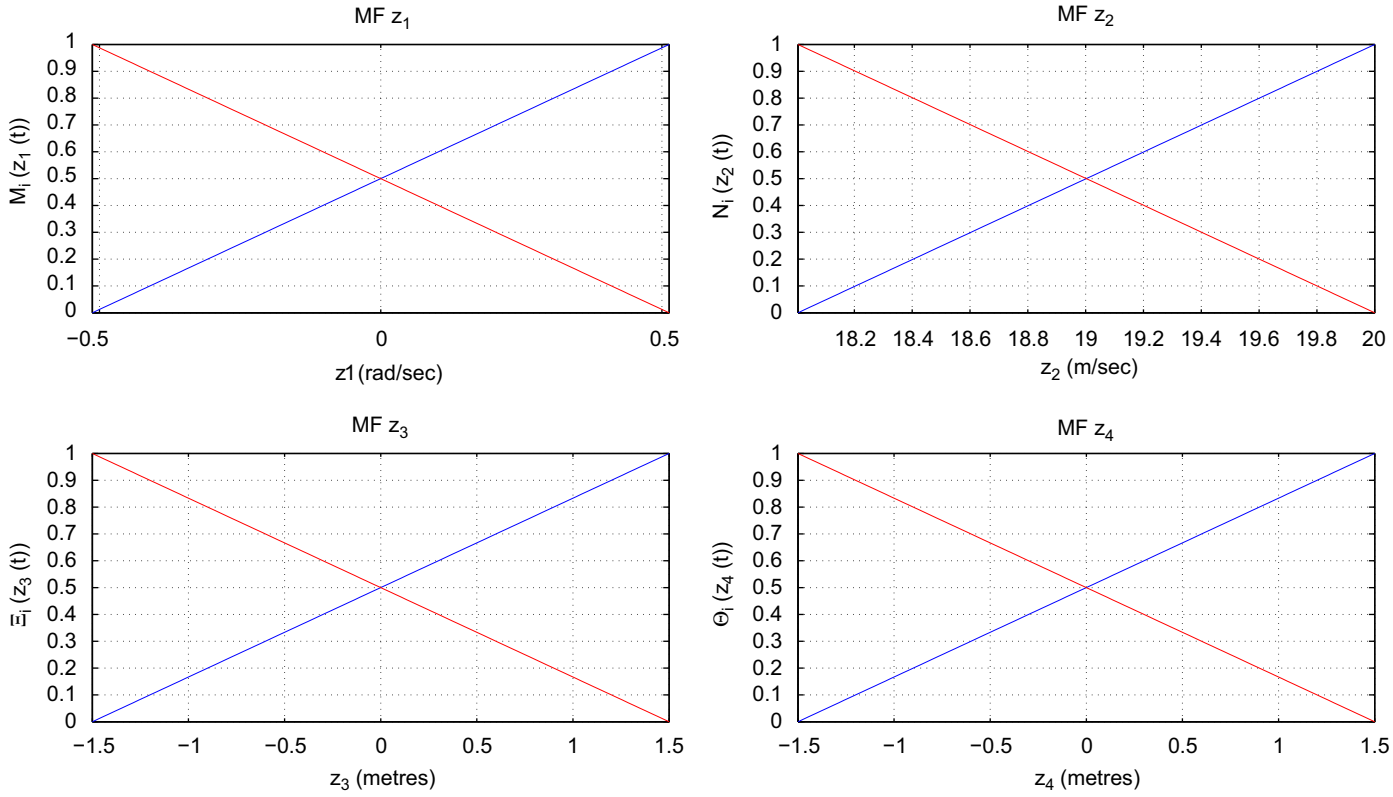

Fig. 10. Membership functions $O_i(z_j(t))$ for z_1, z_2, z_3 and z_4, respectively, representing the degree of truth of $z_j(t)$ in set O_i with saturation points not shown. Alpha cuts of the membership functions chosen in 50%.

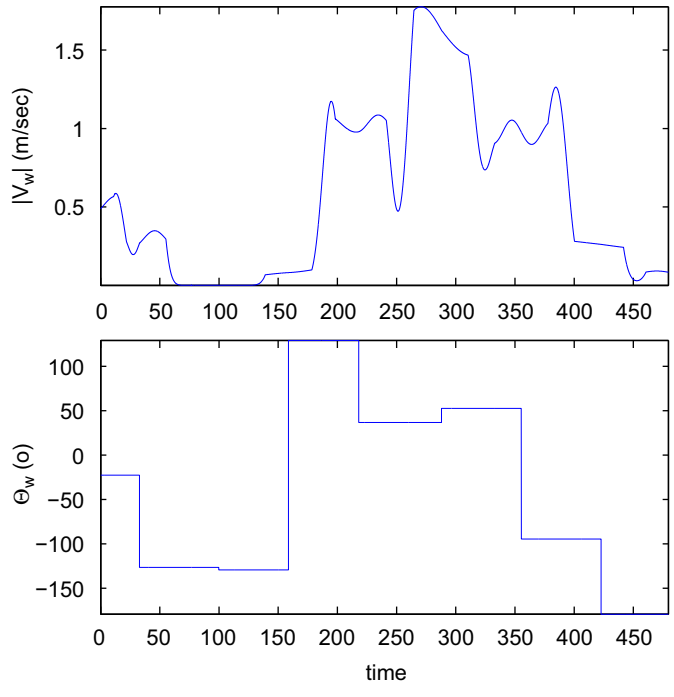

Fig. 11. Magnitude (top) and direction (bottom) of wind for the optimum energy path with respect to time of flight.

the global frame the ones depicted in Fig. 5, respectively, for the entire map. For the path returned in the previous section the magnitude and direction of wind coincide with Fig. 11. Additionally, the initial conditions for the error posture model are $(x_e^{start}, y_e^{start}, \theta_e^{start}) = (0.6, -0.6, 0^\circ)$. The layout of the controller architecture is depicted in Fig. 12. In essence, referring to Fig. 12, the global input to the system are the reference poses and velocities which are varying with respect to time. The global outputs are the current values for the state variables. In other words, the current error posture. The task is for the reference and the current error posture to converge to zero as $t \to \infty$. Finally the current state variables are measured.

The resulting trajectory which is converging to the reference one is depicted in black in Fig. 5. The states of the error posture model coincide with Fig. 13. The smooth *humps* appearing, apart from the peak during initialisation, are due to the wind presence. Notice the nature of the controller that it tries to compensate the additional error appearing. Moreover, referring to Fig. 13, all the states are within the compact region already assumed (dotted solid lines). The latter implies that stability is guaranteed. The means the weighting functions λ_i are firing is depicted in Fig. 14. The premise variables, U_b and U_f coincide with Figs. 15, 16 and 17, respectively. Figs. 18, 19, 20 and 21 depict the heading angle, linear velocity, angular velocity and roll angle calculated versus the reference ones, respectively. It should be noted from Fig. 19 in order to regulate ground velocity the propulsive forces are varying. For instance, for a tailwind (nodes 82–36) the magnitude of the thrust force is decreasing (the velocity is decreasing) and the specific energy is decreasing. Corollary, the power demand is decreasing. In essence there is saving in power (fuel consumed). On the other hand, for a head wind (nodes 90–82), propulsive forces are increased to maintain ground speed and the power demand is increasing (the velocity is increasing). The latter depicts the energy saving nature of the tracking module. It should be mentioned that although convergence can be guaranteed then due to discontinuities in the Dubins path the convergence of the states of the error posture might not be performed in a smooth manner, when wind conditions

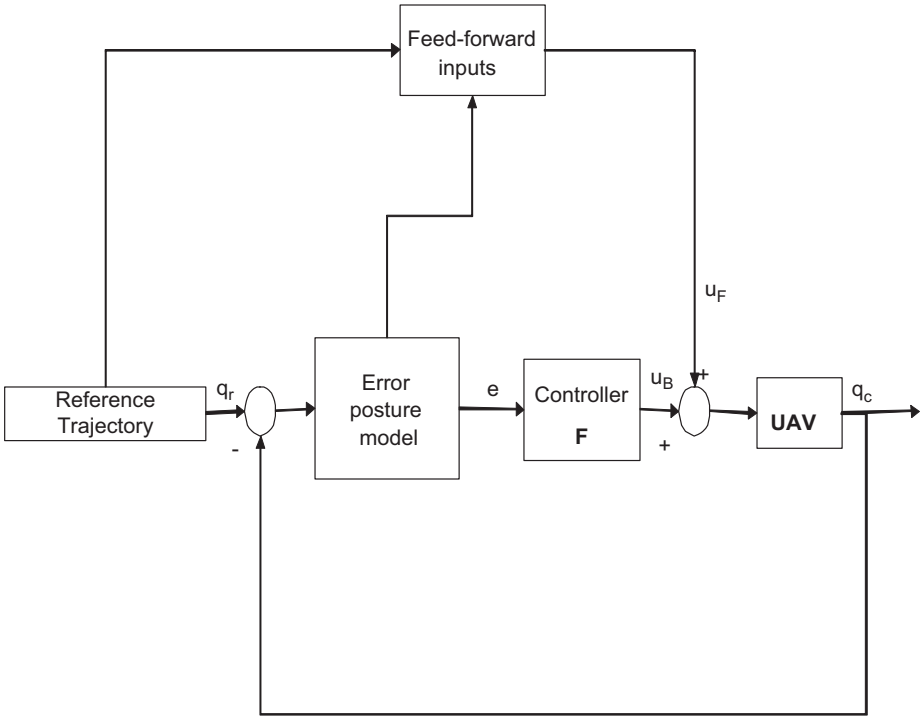

Fig. 12. Architecture of the feed-forward state feedback T–S fuzzy controller.

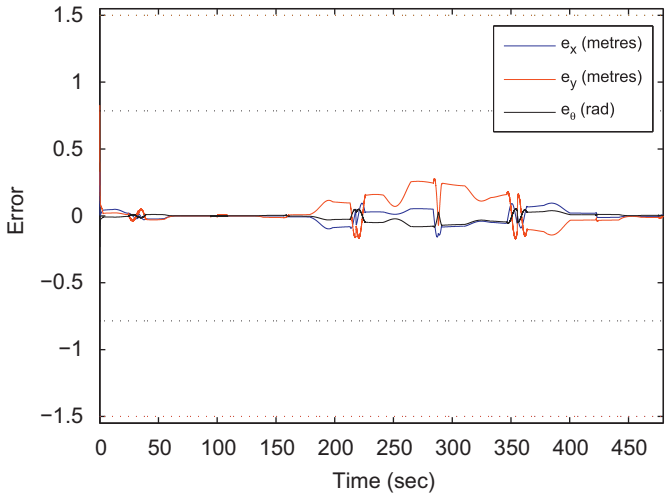

Fig. 13. Convergence of the error dynamics (x_e, y_e, θ_e) of the T–S fuzzy model.

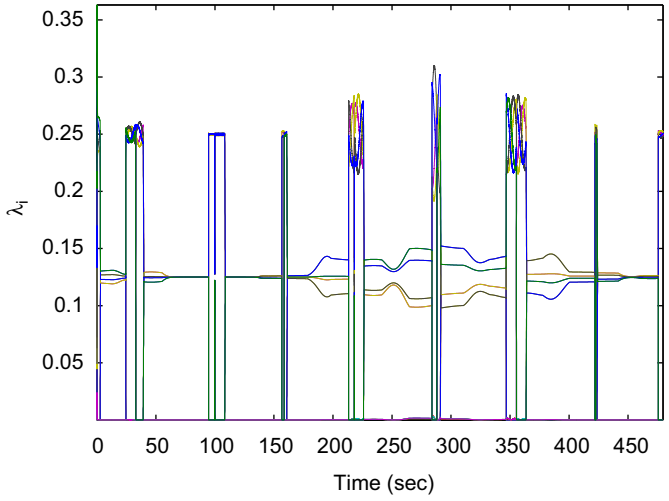

Fig. 14. Weighting functions λ_i for the T–S fuzzy model as calculated from Eq. (18).

are not present. In essence the discontinuities are appearing in the points where the pattern changes from linear to circular segment and otherwise. Hence, a change in direction induces lateral acceleration acting along the tangent by perpendicular means, which cannot be handled directly by the Dubins path unless the UAV reduced its speed while approaching the arc from the line and vice versa. Thus, a sudden change in acceleration will occur, which is not desirable and smoothness of the path should be taken into account which is beyond this analysis. A "naive" alternative is to use another type of trajectory such as a more generalised cubic spline. Nonetheless the latter has its trade offs with respect to path length, minimum time paths, existence of the path due to physical or functional limitations of the aircraft. The latter was illustrated by Shanmugavel (2007).

Finally, the energy requirements and velocity profile for the actual, ground and wind speed are depicted in Fig. 22. Notice that for the calculation of the specific energy demand the mass of the vehicle is not a prerequisite.

The roll angle calculated coincides with the angle demand for the point mass aerial vehicle to track the reference trajectory. This implies that frequency of the roll angle (Fig. 21) does not necessarily mean realistic bank angle demands for the UAV since the vehicle model considered is a point mass one. However, it should be mentioned that the performance or response of the controller can be tuned according to physical and functional limitations of the vehicle considered. The latter can be easily performed by optimising, tuning or assigning realistic values (according to specifications of the particular UAV involved) to the parameters α and μ in LMI conditions (23) and (26), respectively. It is worth noting that tuning the previous parameters sacrifices the performance of the system. It may be worthy of research into the inclusion of delay, bias or degradation to the

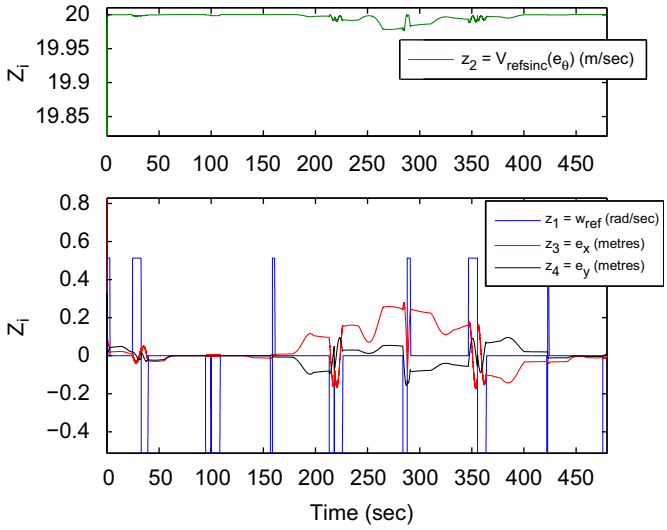

Fig. 15. Premise variables $z_1(t)$, $z_2(t)$, $z_3(t)$ and $z_4(t)$, respectively.

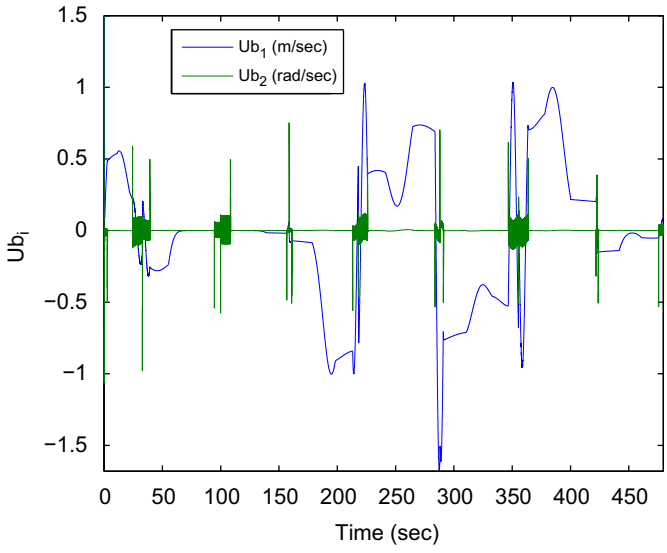

Fig. 16. U_b-state feedback control action vector.

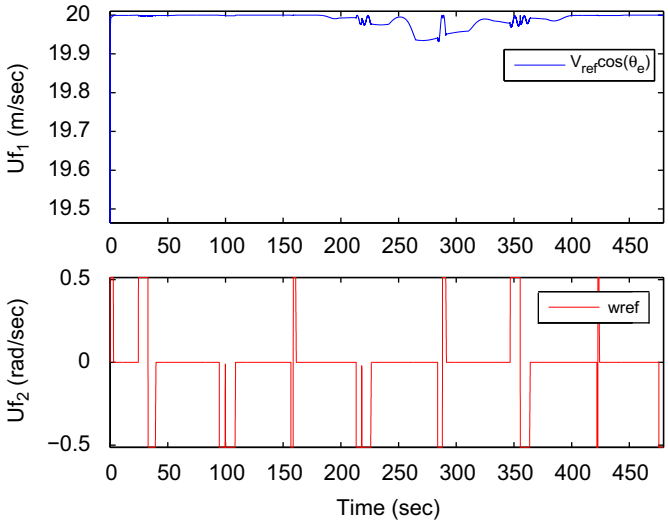

Fig. 17. U_f-feed-forward control action vector.

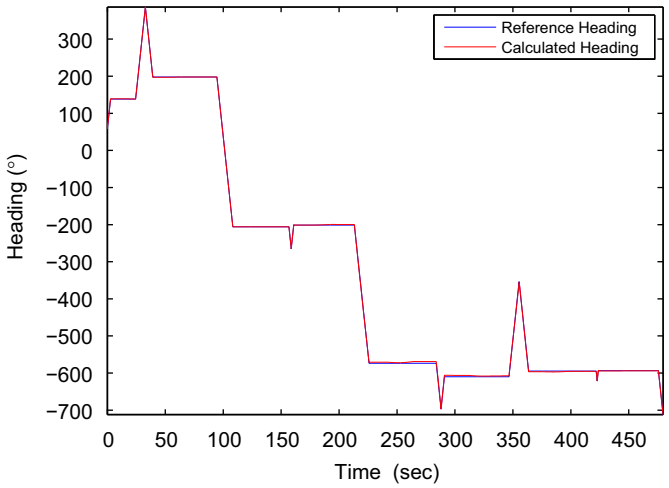

Fig. 18. Calculated and reference heading angle profiles for the optimum energy path.

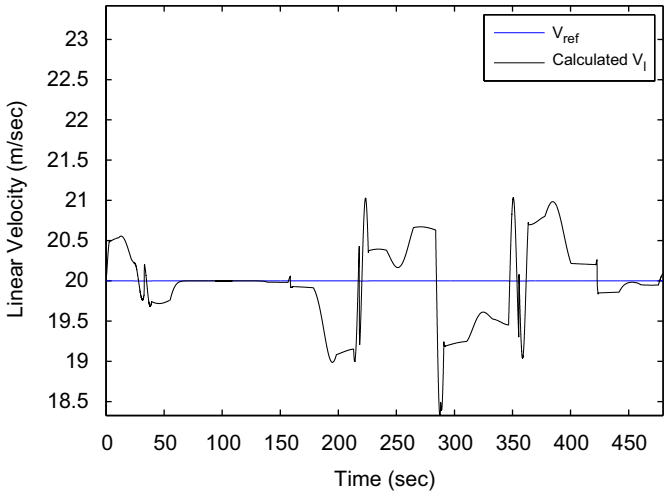

Fig. 19. Calculated and reference linear velocity profiles for the optimum energy path.

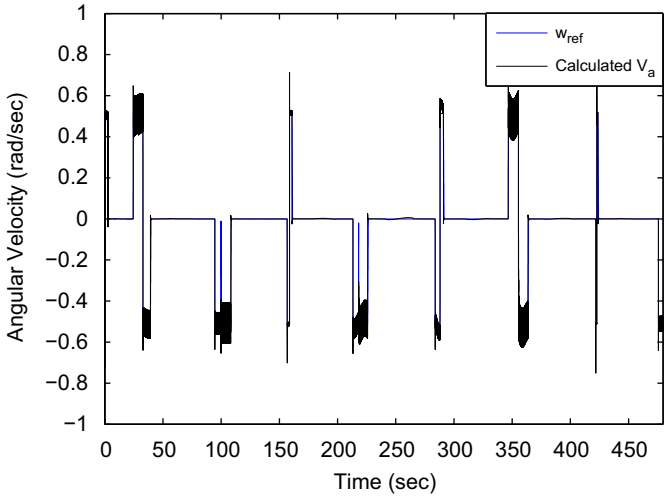

Fig. 20. Calculated and reference angular velocity profiles for the optimum energy path.

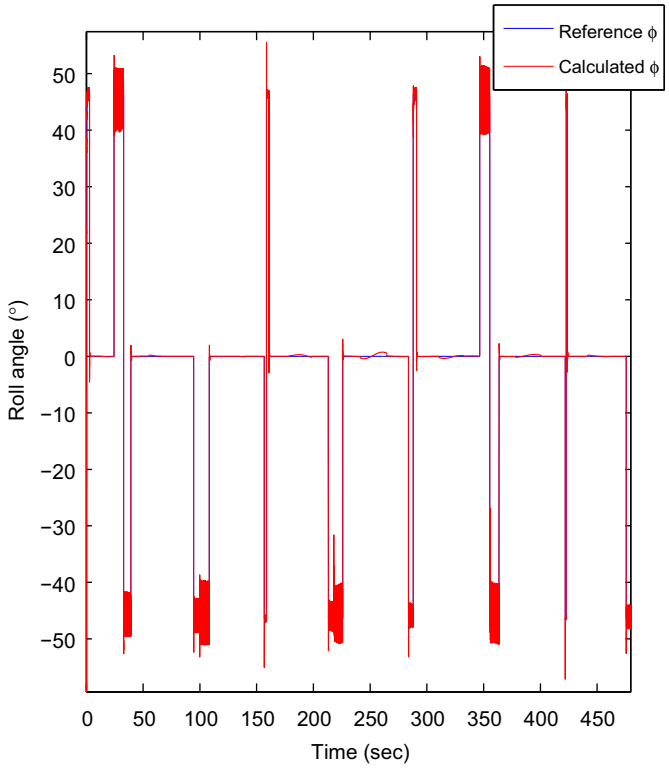

Fig. 21. Calculated and reference roll angles for the optimum energy path.

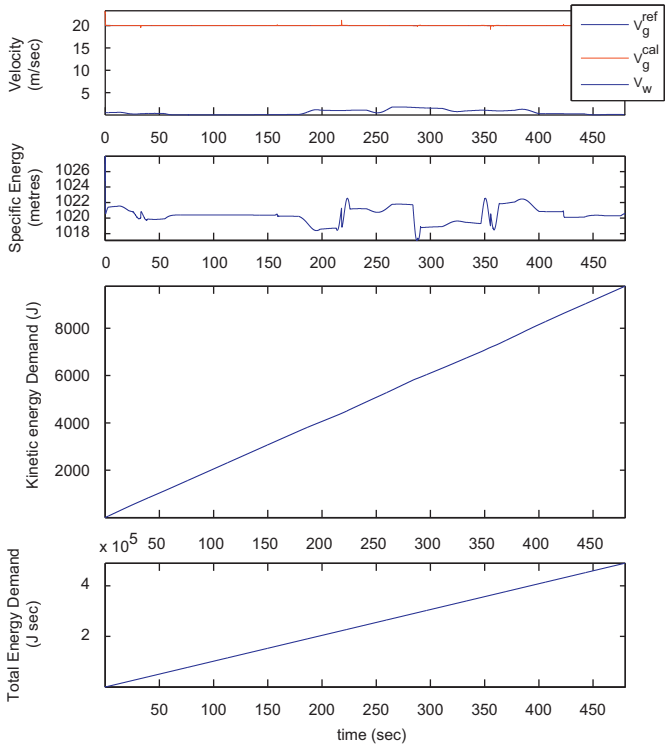

Fig. 22. Calculated energy profile for the mission. From top to bottom: reference ground velocity profile (blue) and calculated one (red), wind velocity (black); specific energy demand for the mission; overall kinetic energy; and total energy profile for the entire mission. (For interpretation of the references to colour in this figure legend, the reader is referred to the web version of this article.)

inputs of the system enforced throughout the time horizon. The latter can be case sensitive with respect to the UAV deployed for the mission and since it is beyond this analysis may be worthy of investigation in future work. Additionally the feedback gains were calculated using global design criteria, thus tracking is guaranteed provided that angular and linear velocities and wind profile properties are bounded. However, practical control applications are often dictated by uncertainties associated with parameters of the system. Robust control addresses those uncertainties and aims to derive the best design possible under such regimes. It may be worth investigating this in future work.

5. Conclusion

In this work a methodology outlined means of determining energy optimum routes for UAV missions when flying under windy conditions. This article is contributing towards energy-enhancing a UAV mission and generating safely-flyable trajectories to meet mission objectives. The control law used is calculated in the pre-flight planning and can be used in real time for any trajectory to be tracked under bounded environmental conditions a priori assumed. Additionally, it offers an improved visualisation to aid an analyst with the representation of a UAV mission through graph theory tools utilising energy requirements for the mission and fast computational schema using matrix analysis.

Graph theory tools were utilised and through their properties their advantages were shown, thus strengthening their use in the UAV context. Furthermore, physical and functional limitations of the vehicle were also included to explain the means to reach a destination node from a source. The standard type of path that yields the navigation step was the Dubins path. The aim of the problem was tracking the Dubins path when wind disturbances are present while in flight. Furthermore, the energy requirements were described and determined in order to complete the mission objectives.

The methodology was illustrated through a simulation scenario. In essence, the UAV is flying under known environmental conditions and the task is to track a predefined planar trajectory while conserving energy requirements and satisfying mission constraints. The routing problem addressed was the classic shortest path problem. Hence, the latter resulted in the determination of a safely-flyable energy-optimum route via the help of shortest path algorithms. Particularly, the Dijkstra algorithm was utilised due to the application domain considered.

For the tracking module the actual horizon motion of the vehicle was described by a Tagaki–Sugeno (T–S) fuzzy system. Additionally, the advantages of utilising such an analysis were also stressed. The model formulated was an error posture model, that depends on current and reference postures. The control law was designed through parallel distributed compensation (PDC) and the feedback gains were computed with the help of linear matrix inequalities (LMIs). Hence stability for the system was also guaranteed provided that the state variables were bounded in an a priori known compact space.

It should be noted from Fig. 19 in order to regulate ground velocity the propulsive forces are varying. For instance, for a tailwind (nodes 82–36) the magnitude of the thrust force is decreasing (the velocity is decreasing) and the specific energy is decreasing. The latter depicts the energy saving nature of the tracking module.

Appendix

Gains $\mathbf{F}_i$ calculated when a known varying wind profile is considered as illustrated in the simulation scenario in Section 4.3:

$$\mathbf{F}_1 = \begin{bmatrix} -11.0418 & -0.5491 & 1.0487 \\ -6.4200 & -38.9284 & -128.9314 \end{bmatrix}$$

$$\mathbf{F}_2=\begin{bmatrix}-10.5480 & 1.2915 & 8.3595\\ -6.6988 & -38.1380 & -125.0319\end{bmatrix}$$

$$\mathbf{F}_3=\begin{bmatrix}-6.9463 & -6.7006 & 1.4402\\ -7.8353 & -39.7937 & -132.4052\end{bmatrix}$$

$$\mathbf{F}_4=\begin{bmatrix}-11.1324 & 4.4041 & 11.2234\\ -7.2448 & -38.2460 & -125.9127\end{bmatrix}$$

$$\mathbf{F}_5=\begin{bmatrix}-11.5937 & -1.4159 & -4.5521\\ -6.0272 & -41.0836 & -134.6327\end{bmatrix}$$

$$\mathbf{F}_6=\begin{bmatrix}-11.1880 & -0.2806 & 0.7908\\ -6.4505 & -39.7213 & -131.2228\end{bmatrix}$$

$$\mathbf{F}_7=\begin{bmatrix}-9.7021 & -3.6882 & 0.4845\\ -7.0443 & -41.2854 & -136.0647\end{bmatrix}$$

$$\mathbf{F}_8=\begin{bmatrix}-11.5562 & 3.3482 & 5.4464\\ -6.9824 & -39.6319 & -131.5261\end{bmatrix}$$

$$\mathbf{F}_9=\begin{bmatrix}-11.4891 & -1.0214 & -2.7823\\ -6.1281 & -40.7416 & -133.7204\end{bmatrix}$$

$$\mathbf{F}_{10}=\begin{bmatrix}-10.8795 & -0.4850 & 2.3254\\ -6.5019 & -39.6565 & -130.5668\end{bmatrix}$$

$$\mathbf{F}_{11}=\begin{bmatrix}-9.0090 & -5.8926 & -2.8594\\ -6.7785 & -41.0787 & -135.3648\end{bmatrix}$$

$$\mathbf{F}_{12}=\begin{bmatrix}-11.4289 & 2.9386 & 6.0235\\ -6.9851 & -39.6122 & -130.9488\end{bmatrix}$$

$$\mathbf{F}_{13}=\begin{bmatrix}-11.7558 & -1.6962 & -6.2239\\ -5.8443 & -41.1998 & -134.8162\end{bmatrix}$$

$$\mathbf{F}_{14}=\begin{bmatrix}-11.2578 & -0.9433 & -1.0926\\ -6.3085 & -39.7258 & -131.4610\end{bmatrix}$$

$$\mathbf{F}_{15}=\begin{bmatrix}-10.4184 & -2.8455 & -0.6437\\ -6.8303 & -41.3411 & -136.1138\end{bmatrix}$$

and

$$\mathbf{F}_{16}=\begin{bmatrix}-11.6138 & 2.6914 & 3.8406\\ -6.8529 & -39.6379 & -131.7980\end{bmatrix}$$

The state $\mathbf{A}_i$, input $\mathbf{B}_i$ and output $\mathbf{C}_i$ matrices are equal to

$$\mathbf{A}_1=\mathbf{A}_2=\mathbf{A}_3=\mathbf{A}_4=\begin{bmatrix}0 & -0.5128 & 0\\ 0.5128 & 0 & 18.0048\\ 0 & 0 & 0\end{bmatrix}$$

$$\mathbf{A}_5=\mathbf{A}_6=\mathbf{A}_7=\mathbf{A}_8=\begin{bmatrix}0 & -0.5128 & 0\\ 0.5128 & 0 & 20\\ 0 & 0 & 0\end{bmatrix}$$

$$\mathbf{A}_9=\mathbf{A}_{10}=\mathbf{A}_{11}=\mathbf{A}_{12}=\begin{bmatrix}0 & 0.5128 & 0\\ -0.5128 & 0 & 18.0048\\ 0 & 0 & 0\end{bmatrix}$$

$$\mathbf{A}_{13}=\mathbf{A}_{14}=\mathbf{A}_{15}=\mathbf{A}_{16}=\begin{bmatrix}0 & 0.5128 & 0\\ -0.5128 & 0 & 20\\ 0 & 0 & 0\end{bmatrix}$$

$$\mathbf{B}_1=\mathbf{B}_5=\mathbf{B}_9=\mathbf{B}_{13}=\begin{bmatrix}-1 & -1.5\\ 0 & 1.5\\ 0 & -1\end{bmatrix}$$

$$\mathbf{B}_2=\mathbf{B}_6=\mathbf{B}_{10}=\mathbf{B}_{14}=\begin{bmatrix}-1 & -1.5\\ 0 & -1.5\\ 0 & -1\end{bmatrix}$$

$$\mathbf{B}_3=\mathbf{B}_7=\mathbf{B}_{11}=\mathbf{B}_{15}=\begin{bmatrix}-1 & 1.5\\ 0 & 1.5\\ 0 & -1\end{bmatrix}$$

$$\mathbf{B}_4=\mathbf{B}_8=\mathbf{B}_{12}=\mathbf{B}_{16}=\begin{bmatrix}-1 & 1.5\\ 0 & -1.5\\ 0 & -1\end{bmatrix}\quad\text{and}\quad\mathbf{C}_i=\begin{bmatrix}1 & 0 & 0\\ 0 & 1 & 0\\ 0 & 0 & 1\end{bmatrix}$$

$\forall i=1,\ldots,16$ and $i\in\mathbb{N}^+$

References

Allison, R., Hedrick, J.K., 2005. A mode-switching path planner for UAV-assisted search and rescue. In: 44th IEEE Conference on Decision and Control, and the European Control Conference, CDC-ECC '05, pp. 1471–1476.

Bernal, M., Guerra, T.M., Kruszewski, A., 2009. A membership-function-dependent approach for stability analysis and controller synthesis of Takagi–Sugeno models. Fuzzy Sets and Systems 160 (19), 2776–2795.

Boyd, S., El Ghaoui, L., Féron, E., Balakrishnan, V., 1994. Linear Matrix Inequalities in System and Control Theory. Studies in Applied Mathematics, Philadelphia.

Christofides, N., 1975. Graph Theory an Algorithmic Approach. Academic Press INC, (London) LTD.

Dijkstra, E.W., 1959. A note on two problems in connexion with graphs. Institut für Numerische Mathematik 1, 269–271.

Dubins, L.E., 1957. On curves of minimal length with a constraint on average curvature and with prescribed initial and terminal positions and tangent. American Journal of Mathematics 79, 497–516.

Economou, J.T., Kladis, G.P., Tsourdos, A., White, B.A., 2007a. UAV optimum energy assignment using Dijkstra algorithm. In: European Control Conference, ECC 2007, Kos, Greece, July, 2–5th.

Economou, J.T., Colyer, R.E., Zbikowski, R.W., 1999. Electric rotary actuator sizing applied to wheeled skid-steer vehicles. Proceedings of the 38th IEEE Conference on Decision and Control, 1999, vol. 5; 1999, pp. 5271–5276.

Economou, J.T., Kladis, G.P., Tsourdos, A., White, B.A., 2007b. A node-to-node composite graph and pseudo-boolean modeling: a UAV energy application. Journal of Aerospace Engineering. Part G: Proceedings of the Institution of Mechanical Engineering 221 (5), 815–830.

Fliess, M., Martin, L.J.P., Rouchon, P., 1995. Flatness and defect of nonlinear systems: introductory theory and examples. International Journal of Control 61 (6), 1327–1361.

Guerra, T.M., Vermeiren, L., 2004. LMI-based relaxed non-quadratic stabilization conditions for nonlinear systems in the Takagi–Sugeno's form. Automatica 40 (5), 823–829.

Guerra, T.M., Kruszewski, A., Vermeiren, L., Tirmant, H., 2006. Conditions of output stabilization for nonlinear models in the Takagi–Sugeno form. Fuzzy Sets and Systems 157 (9), 1248–1259.

Kawamoto, S., Tada, K., Ishigame, A., Taniguchi, T., 1992. An approach to stability analysis of second order fuzzy systems. In: Proceedings of First IEEE International Conference on Fuzzy Systems, vol. 1, pp. 1427–1434.

Kanayama, Y., Kimura, Y., Miyazaki, F., Noguchi, T., 1991. A stable tracking control method for a non-holonomic mobile robot. In: IEEE/RSJ International Workshop on Intelligent Robots and Systems IROS '91, vol. 3, Osaka, Japan, pp. 1236–1241.

Kladis, G.P., 2010. Autonomous multi-agent aerial vehicle systems utilising energy requirements, Ph.D. Dissertation, Department of Engineering Systems and Management, Defense College of Management and Technology of the United Kingdom, Cranfield University, Shrivenham, Swindon, Wiltshire, UK, March.

Kladis, G.P., Economou, J.T., Tsourdos, A., White, B.A., Knowles, K., 2008a. An emergency refueling problem over a dynamically changing environment in the context of unmanned aerial vehicles. In: 2008 16th Mediterranean Conference on Control and Automation, MED 2008, 25–27th June 2008, Corsica, France, pp. 703–708.

Kladis, G.P., Economou, J.T., Tsourdos, A., White, B.A., 2007. Optimality and reachability—pseudo boolean power flows for a multi-sourced vehicle topologies. In: IEEE 2007 Vehicle Power and Propulsion Conference, VPPC 2007, 9–12th September, Arlinghton, Texas, USA, pp. 808–813.

Kladis, G.P., Economou, J.T., Tsourdos, A., White, B.A., Knowles, K., 2008b. Aerospace energy conservation utilising optimum methods. In: IEEE 2008 Vehicle Power and Propulsion Conference, VPPC 2008, 3–5th September, Harbin, China, pp. 1–6.

Khiar, D., Lauber, J., Floquet, T., Colin, G., Guerra, T.M., Chamaillard, Y., 2007. Robust Takagi–Sugeno fuzzy control of a spark ignition engine. Control Engineering Practice 15 (12), 1446–1456.

Klančar, G., Skrjanc, I., 2007. Tracking-error model-based predictive control for mobile robots in real time. Robotics and Autonomous Systems 55 (3), 460–469.

Laumond, J.P., 1998. Robot motion planning and control. In: Lecture Notes in Computer Science, vol. 229. Springer.

Liu, X., Zhang, Q., 2003. New approaches to controller designs based on fuzzy observers for Takagi–Sugeno fuzzy systems via LMI. Automatica 39 (9), 1571–1582.

Nelson, W., Cox, L., 1988. Local path control for an autonomous vehicles. In: Proceedings of the IEEE International Conference on Robotics and Automation, pp. 1504–1510.

Rathinam, S., Sengupta, R., 2004a. A safe flight algorithm for unmanned aerial vehicles. IEEE Aerospace Conference Proceedings 5 (6), 3031–3041.
Rathinam, S., Sengupta, R., 2004b. Safe UAV navigation with sensor processing delays in an unknown environment. In: 43rd IEEE Conference on Decision and Control (CDC), vol. 1, no. 1, 2004, pp. 1081–1086.
Richards, A., How, J.P., 2002. Aircraft trajectory planning with collision avoidance using mixed integer linear programming. In: American Control Conference, 2002. Proceedings of the 2002, vol. 3, pp. 1936–1941.
Sala, A., Ariño, C., 2007. Asymptotically necessary and sufficient conditions for stability and performance in fuzzy control: applications of polya's theorem. Fuzzy Sets and Systems 158, 2671–2686.
Shanmugavel, M., 2007. Path planning of multiple autonomous vehicles. Ph.D. Dissertation, Department of Aerospace, Power and Sensors, Cranfield University, Shrivenham, Swindon, Wiltshire, UK, May.
Stevens, B., Lewis, F., 1992. Aircraft Control and Simulation. Wiley, NY.
Sugeno, M., Kang, G.T., 1986. Structure identification of fuzzy model. Fuzzy Sets and Systems 28, 329–346.
Takagi, T., Sugeno, M., 1985. Fuzzy identification of systems and its application to modeling and control. IEEE Transactions on System Man and Cybernetics 15 (1), 116–132.
Tanaka, K., Wang, H.O., 2001. Fuzzy Control Systems Design and Analysis: A Linear Matrix Inequality Approach. John Wiley and Sons, Inc, New York.
Tanaka, K., Ikeda, T., Wang, H.O., 1996. Robust stabilization of a class of uncertain nonlinear system via fuzzy control: quadratic stabilizability, H infinity control theory and linear matrix. IEEE Transactions on Fuzzy Systems 4, 1–13.
Tennekes, H., 1996. The Simple Science of Flight. MIT Press, Cambridge, MA.
Tuan, H.D., Apkarian, P., Narikiyo, T., Yamamoto, Y., 2001. Parameterized linear matrix inequality techniques in fuzzy control system design. IEEE Transactions on Fuzzy Systems 9 (2), 324–332.
Wang, H.O., Tanaka, K., Griffin, M.F., 1995. Parallel distributed compensation of nonlinear systems by Takagi–Sugeno fuzzy model. In: Proceedings of the FUZZ-IEEE/IFES'95, pp. 531–538.
Vinh, N.X., 1995. Flight Mechanics of High-performance Aircraft, series 5. Cambridge University Press, Cambridge, United Kingdom (Cambridge Aerospace Series).